GEOPHYSICS, VOL. 68, NO. 1 (JANUARY-FEBRUARY 2003); P. 70–91, 23 FIGS., 4 TABLES.
10.1190/1.1543195

## Case History

# Okak Bay AMT data-set case study: Lessons in dimensionality and scale

Alan G. Jones* and Xavier Garcia‡

**ABSTRACT**

Electromagnetic (EM) exploration for base metals using the natural-source audio-magnetotelluric (AMT) technique has increased significantly during the last five years due to enhancements in all aspects of AMT and to the demand for imaging deeper than conventional controlled-source EM methods. However, regional currents induced by natural sources can be problematic in certain situations, and the appropriate interpretational dimensionality must be known. Herein we demonstrate that a two-dimensional (2D) interpretation is valid for a defined frequency band, but that the effects of large-scale three-dimensional (3D) structures must be considered at lower frequencies. Using an AMT dataset from an area located north of Voisey's Bay, Labrador, Canada, we analyse the responses to determine the appropriate dimensionality and to test them for internal consistency. Maps of the distortion-corrected data identify the lateral extent of connected conducting mineralization intersected by a drilling program. One-dimensional (1D) inversions of the corrected data from those sites on top of the mineralized zone show the resolution properties of the data. We constructed a pseudo-3D model from 2D inversions of the data in the frequency band 1000–10 Hz from all profiles, and this model images the mineralized body sufficiently for exploration purposes. We suggest that the anomalous low-frequency responses observed at sites close to the mineralized zone are possibly due to charges impinged on the mineralized body's boundaries by currents induced in the Atlantic Ocean some 50 km away. Although 3D numerical modeling studies exhibit some of the effects observed, we are unable to reproduce numerically the observed behavior.

## INTRODUCTION

Exploration for economic mineralization in mature prospects in Canada is focused on using geophysical methods that probe deeper than conventional techniques (i.e., >500 m). For electromagnetic surveys, the natural-source audio-magnetotelluric method (AMT) has become an attractive option with its ability to image conductivity structures in resistive basement from about 300 m to a few kilometers. Controlled-source AMT (CSAMT), proposed in the mid-1970s (Goldstein and Strangway, 1975) to counter the poor and unreliable natural-source AMT data acquired at that time, has been used extensively in the past but suffers from more involved and complex logistical requirements (a bipole source), typically lack of tensor information, fewer processing, analysis, and modeling tools, and a restricted physical range of valid application. Understanding the nature of the natural source fields (Garcia and Jones, 2002) together with developments in instrumentation, processing, analysis, modeling, and inversion have recently led to preferential use of AMT over CSAMT in Canada for both regional exploration activities and for anomaly delineation. Large AMT surveys, principally for base metals, have been conducted since 1996 in Newfoundland (Voisey's Bay), Ontario (Sudbury basin), and Manitoba (Thompson nickel belt), with more than 15 000 AMT sites acquired in Canada (see, e.g., Livelybrooks et al., 1996; Chouteau et al., 1997; Balch et al., 1998; Stevens and McNeice, 1998; Zhang et al., 1998).

A relatively small (46 sites) AMT survey was conducted over a magnetic high north of the renowned Voisey's Bay deposit,

Manuscript received by the Editor September 18, 2000; revised manuscript received January 02, 2002.
*Geological Survey of Canada, Continental Geoscience Division, 615 Booth Street, Room 218, Ottawa, Ontario K1A 0E9, Canada. E-mail: ajones@nrcan.gc.ca.
‡Formerly Geological Survey of Canada, Continental Geoscience Division, Ottawa, Ontario, Canada; presently Woods Hole Oceanographic Institution, Woods Hole, Massachusetts 02543. E-mail: xgarcia@whoi.edu.

and preliminary interpretation of the AMT data prompted a drilling program to more than 1.5-km total depth extent. Weak mineralization was intersected at ~500-m depth, as expected from the interpretation, but a far larger anomaly, expected at approximately 1-km depth based on the modeling, was not intersected. Using modern analytical methods, two-dimensional (2D) inversions, and three-dimensional (3D) regional-scale modeling, we have undertaken a more complete interpretation of the data in order to gain knowledge about appropriate interpretative techniques and to provide a more comprehensive model of the conductivity structure of the body and of the surrounding region.

This case study describes our approach to data analysis and interpretation, and demonstrates that under appropriate circumstances a 2D assumption about the subsurface may be valid. However, we also demonstrate that a complete understanding of the regional current flow is necessary to interpret the observations correctly, and that large-scale regional 3D structures can dramatically influence observations in a non-intuitive manner.

## OKAK BAY AMT SURVEY

### Regional setting

Okak Bay is a small inlet in the northern Labrador coast 100 km north of the spectacular world-class Voisey's Bay nickel deposit (Figure 1), and the area of interest lies within National Topographic System (NTS) 1:250K map sheet 14 E/07 (Umiakovik Lake). The regional-scale geology shown on Figure 1 (insert) comes from the Wheeler et al. (1997) digital compilation, which, in the survey area, is based on the reconnaissance mapping of Taylor et al. (1969) and compilations of

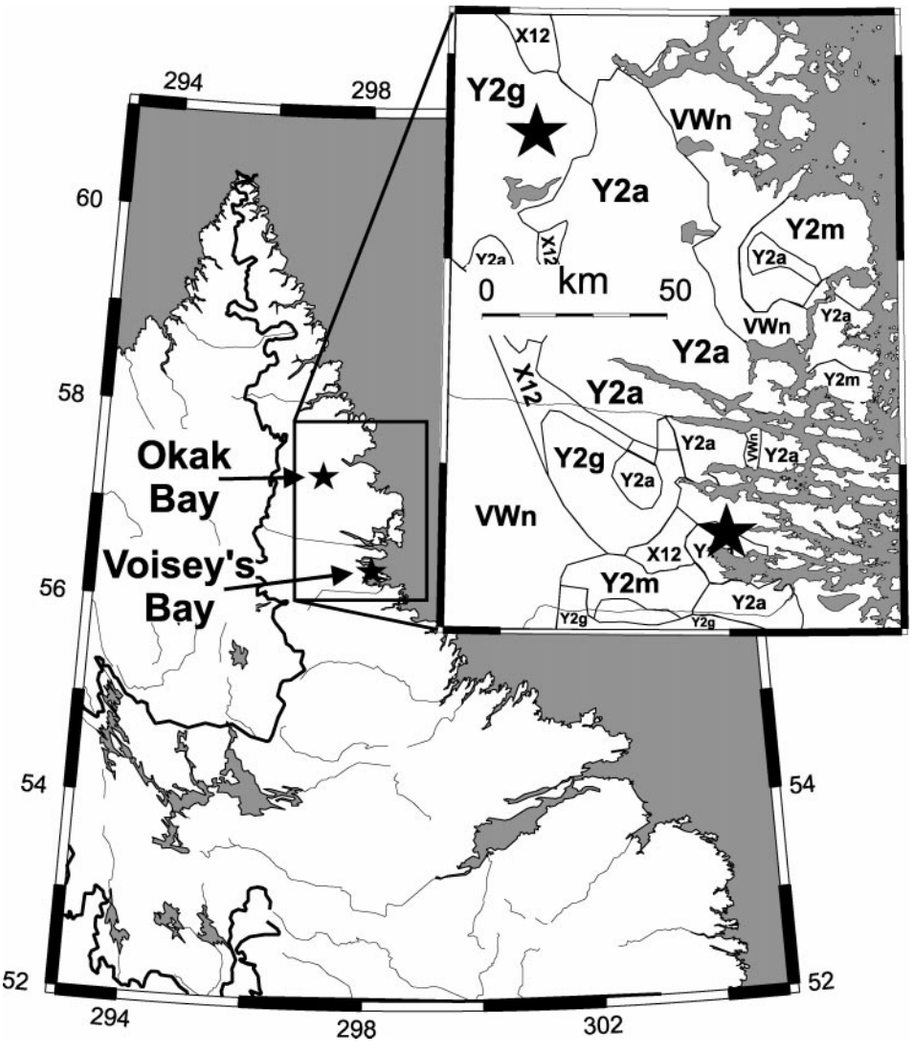


FIG. 1. Map of northern Labrador, eastern Canada, showing the locations of the Okak Bay deposit and the Voisey's Bay deposit. Insert: Local setting of Okak Bay and Voisey's Bay deposits with the regional geological mapping from Wheeler et al. (1997). *Y2g*: undivided Mesoproterozoic intrusive granitoid rocks (locally, the Umiakovik Lake batholith); *Y2a*: Mesoproterozoic anorthosite; *VWn*: undivided Mesoarchean-Neoarchean metamorphic rocks; *X12*: undivided Paleoproterozoic sedimentary rocks. For other units, see Wheeler et al. (1997).

Taylor (1977) and Ryan (1990). The area is in the Mesoarchean Nain craton of Labrador, east of the Paleoproterozoic Torngat orogen. Modern detailed mapping by Ermanovics and colleagues, reported in Ermanovics et al. (1997) and Ermanovics and van Kranendonk (1998), occurred to the north and east of the survey area. On the regional maps, the survey was entirely within the Umiakovik Lake batholith mapped by Taylor (1977), predominantly a pyroxene-hornblende quartz monzonite (Ermanovics et al., 1997; Ermanovics and van Kranendonk, 1998) dated as a circa 1320 Ma intrusion (Emslie and Loveridge, 1992). No public-domain detailed geological mapping information currently exists for the survey area, which lies some 10 km directly south of Umiakovik Lake.

Attention was drawn to the Okak Bay area in 1995 by the existence of a magnetic high some 25 km inland from the bay. A detailed aeromagnetic survey in 1996 further delineated the extent of the anomaly, and resulted in ground-based geophysical surveys commencing in 1997. These surveys included both regional reconnaissance and targeted AMT measurements in July/August 1997 and a transient electromagnetic (TEM) survey in May 1999.

## AMT data

AMT data were acquired at a total of 46 sites in the frequency band 10 000–1 Hz, and the responses are generally of good quality (small error bars, low scatter) below 1000 Hz. At most sites, the responses cannot be used above 1000 Hz due to the poor magnetic field signal-to-noise ratio in the AMT "dead-band" of 1000–4000 Hz (Garcia and Jones, 2002). This lack of high-quality responses above 1000 Hz is unfortunate because the area of study is located on highly resistive crystalline plutonic rocks and consequently electromagnetic waves penetrate deep into the ground even at high frequencies. For a typical upper crustal resistivity of 10 000 ohm-m, which is the average level of the apparent resistivity curves, at 1000 Hz the natural electromagnetic (EM) waves penetrate to 1500 m (one skin depth), and the depth of maximum eddy current flow (Weidelt, 1972), or depth of investigation (Spies, 1989), is between 600 and 900 m. Accordingly, without data above 1000 Hz, the anomalies in the upper 500 m are detected, but their precise geometries are poorly resolved. For example, for a one-dimensional (1D) earth of 10 000 ohm-m with a 100 ohm-m layer between 250 and 300 m, and with synthetic 2% error data in the frequency band 10 kHz–10 Hz, one can resolve the top of the layer to within ±12 m, whereas if the data are only in the range 1 kHz–10 Hz then the error in the estimate of the top increases to ±29 m.

The dataset has been divided into nine profiles (Figure 2), five oriented north-south (0, 6, 8, 1, 2), three east-west (A, B, C), and one northwest-southeast (Z), and the sites have been assigned to the various profiles for modeling and interpretation.

## Preliminary interpretation

A preliminary 2D model of the data along the main north-south profile (line 6) is shown in Figure 3. This model, from both MT modes data in the frequency band 1000–1 Hz, was derived by the contractor using Smith and Booker's (1991) rapid relaxation inversion (RRI) code and shows small, shallow conductors within 250 m of the surface beneath sites 604 and 616 + 608. However, dominant in the model is the large central conductor of resistivity <100 ohm-m, beginning at a depth of ~1 km and extending to 3 km beneath sites 615–608. Two other anomalies are imaged, one at each end of the line, at about 2 km depth and of resistivity 100–300 ohm-m.

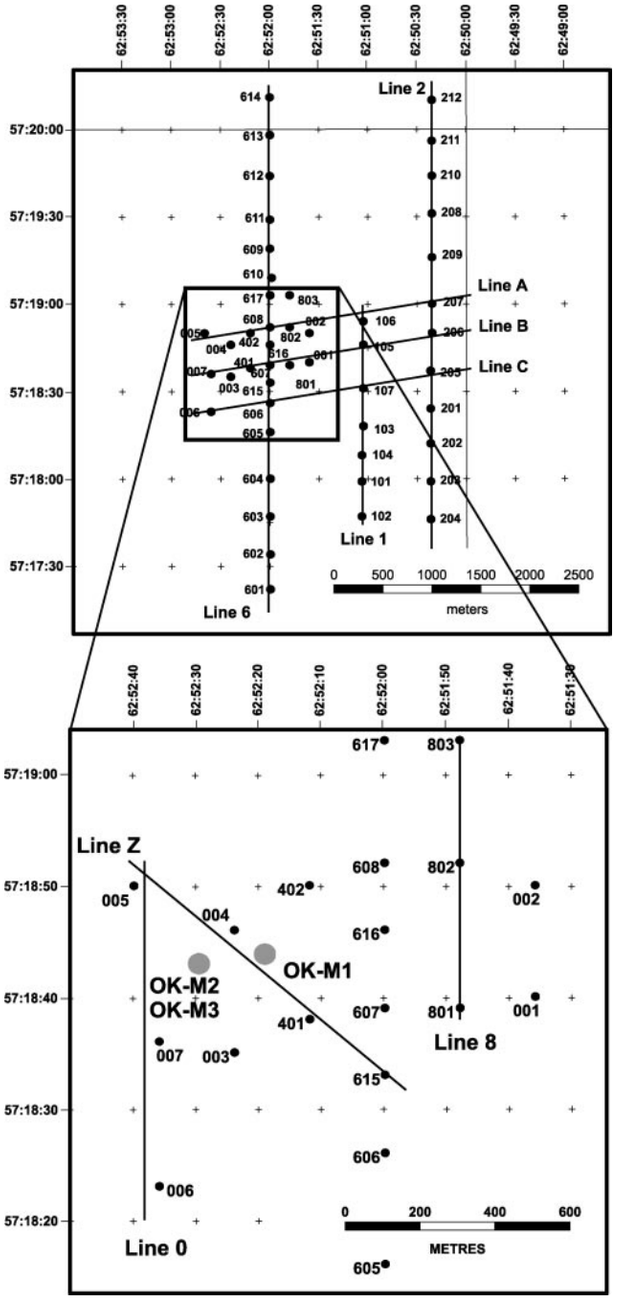


FIG. 2. Map of AMT site locations in the Okak Bay deposit area. The AMT sites were assigned to the nine profiles shown (0, 1, 2, 6, 8, A, B, C, Z). Also shown are the locations of the drillholes OK-M1 and OK-M2/OK-M3.

### Drilling results

Based on the model and the magnetotelluric (MT) responses from the sites to the west of line 6, three boreholes were drilled at the locations shown in Figure 2 as OK-M1 and OK-M2. Hole OK-M2 included a vertical hole (OK-M3) and one drilled at an angle (OK-M2) to intersect OK-M1 at about 750-m depth. Hole OK-M1 was drilled in 1997 to a final depth of 1505 m and, although weakly mineralized zones were intersected at shallower depths, beyond 1001 m the formations comprised predominantly anorthosite with intercalated gabbro. Hole OK-M2, drilled in 1998 with a dip of 73.5°, also found weakly mineralized zones. Hole OK-M3, also drilled in 1998 with a dip of 85°, intersected the zone with the highest mineralization in the depth interval 454.1–470.5 m. A geological log of the hole from 348 to 740 m depth interval is in Table 1.

**Table 1. Geological log of hole OK-M3 in the depth interval 348–740 m.**

| Depth Interval | Description |
|---|---|
| 348.0–449.8 | Minor magnetite local concentrations up to 1–3% |
| 449.8–454.1 | Magnetite-rich gabbro, 8–12% disseminated magnetite, 1/2% disseminated pyrrhotite, and rare chalcopyrite |
| 454.1–470.5 | Gabbro (mineralized zone) 0.5–10% disseminated sulfides, mainly pyrrhotite with minor chalcopyrite |
| 470.5–496.4 | Intercalated gabbro and coarse grained anorthosite, trace magnetite and sulfides |
| 496.4–569.7 | Predominantly coarse-grained anorthosite with lesser leucogabbro; trace to locally 2% magnetite, trace to locally 2% pyrrhotite, and rare chalcopyrite |
| 569.7–589.6 | Fine-grained gabbro, trace magnetite and pyrrhotite |
| 589.6–636.8 | Similar to 496.4–569.7 |
| 636.8–675.3 | Magnetite-rich gabbro, 3–6% disseminated magnetite, 0–1/2% disseminated pyrrhotite, and rare chalcopyrite |
| 675.3–679.3 | Intercalated anorthosite and magnetite-rich gabbro |
| 679.3–740.1 | Anorthosite with narrow lenses of gabbro containing up to 2% magnetite and trace to 1% pyrrhotite and chalcopyrite. Gabbro lenses are less than 1 m wide. |

## DATA ANALYSIS

Subsequent to the drilling results from OK-M1 demonstrating that there were problems with the preliminary interpretation of the AMT data, we were asked to undertake a more comprehensive analysis, modeling, and interpretation. The first steps when interpreting AMT data must always be (1) to understand the inherent dimensionality of the data, (2) to determine the appropriate strike direction for interpretation, and (3) to remove, as much as possible, the effects caused by local, near-surface inhomogeneities. The pitfalls inherent in interpreting AMT data with inappropriate dimensionality have been described by many authors over the last three decades. One-dimensional interpretation of 2D data is known to introduce "false conducting layers" (Berdichevsky and Dmitriev, 1976) at off-anomaly sites, among other artifacts. Two-dimensional interpretation of 3D data can lead to underestimates of the total conductance (Wannamaker et al., 1984; Martinelli et al., 2000), discussed further below. Interpretation in an incorrect coordinate system will yield erroneous structure in the model. Finally, near-surface features distort the regional responses that, if not removed, will also give inaccurate information about the subsurface.

For dimensionality analysis we undertook two studies. The first consisted of calculating phase sensitivity skew (Bahr, 1991), and the second was tensor decomposition using the McNeice and Jones (2001) extended Groom-Bailey (Groom and Bailey, 1989) approach. The final step of our analysis prior to modeling is to test that the data are internally consistent, i.e., that the apparent resistivity and phase curves are compatible with each other as predicted by the spectral expansion of the impedance formalism (Parker and Booker, 1996). Data that are inconsistent cannot be modeled successfully with either 1D or 2D codes, and probably also not with inductive 3D codes (but the Hilbert transform relationship between the amplitude and phase response has yet to be established mathematically).

Once an appropriate strike direction has been defined for the data, then one can obtain the regional impedances in that coordinate system. The responses for electric currents flowing along the structure are termed the transverse-electric (TE) mode, whereas those for currents crossing structures are termed the transverse magnetic (TM) mode.

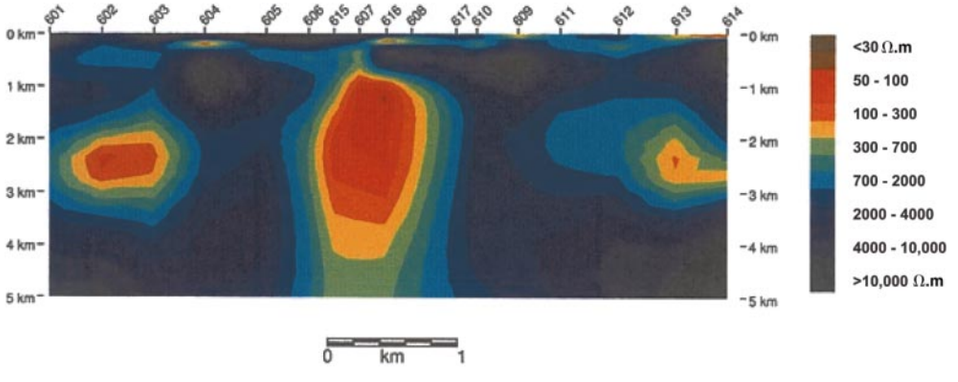


FIG. 3. Preliminary 2D resistivity model of the AMT data from line 6 derived by the contractor (downloaded from the Gallery Resources web site).

### Phase sensitive skew

Phase sensitivity skew (PSS) is a measure of the local 3D distortion of regional 2D fields based on impedance phase, rather than on impedance magnitudes that is the conventional definition of skew (Vozoff, 1972, 1991). According to Bahr (1991), if the value of PSS is greater than 0.3, the data should be considered 3D. We calculated the PSS for the whole data set (Figure 4) and at frequencies above 1000 Hz the PSSs are generally greater than 0.3, but at lower frequencies they are below 0.3. Following Bahr (1991), this would suggest that we can validly undertake a 2D interpretation in the frequency range 1000–~2 Hz, but this needs to be verified statistically taking error information into account.

### Tensor decomposition

An extended version of Groom-Bailey (GB) tensor decomposition (Groom and Bailey, 1989) of the data was used to investigate the dimensionality and to extract the regional 2D impedances corrected for galvanic distortions caused by local, near-surface inhomogeneities. The methodology for GB tensor decomposition is described in Groom et al. (1993) and Jones and Dumas (1993), and the extended multisite, multifrequency approach in McNeice and Jones (2001) (MJ).

Multifrequency MJ tensor decomposition, with bandwidths of one decade, was performed on the data from each site, and maps of the geoelectric strike directions are shown in Figure 5. The lengths of the arrows express how well the decomposition model fits the data at each site and for each decade; long arrows (longest three) indicate a statistically acceptable fit, and short arrows (shortest three) indicate an unacceptable fit. A poor fit can be due to error estimates that are too small (a known problem with parametric error estimates; see Chave and Jones, 1997) or to 3D inductive effects. The map for the highest frequency band (Figure 5a) shows strong site-to-site variation and also small arrows indicating misfit to the galvanic-only distortion model. We interpret this model misfit as caused by the low data quality in this band and to near-surface (<500 m) inhomogeneities causing 3D induction effects. The maps for the next three decades show good site-to-site consistency and acceptable fits, with generally an east-west strike direction for these data.

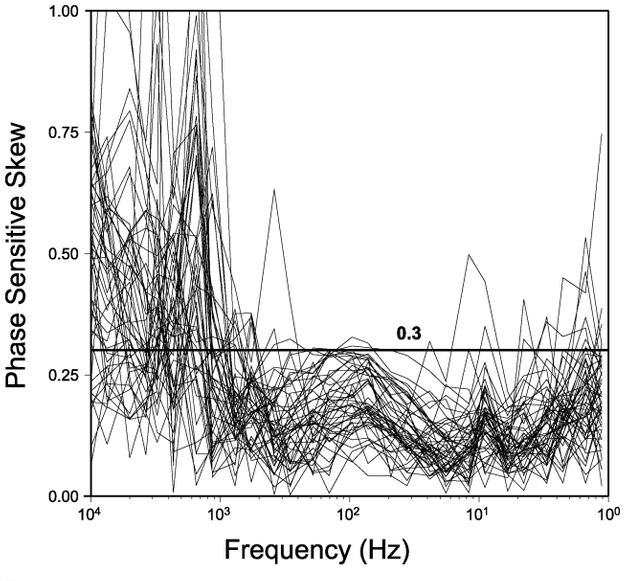


FIG. 4. Phase sensitive skew calculated from the AMT responses at all 48 sites.

The 90° ambiguity in strike direction was resolved by reference to the induction vectors and also by a 3D model study. Test 3D modeling of a spherical body showed that the appropriate strike direction for 2D interpretation is towards the body, i.e., the radial electric field is equivalent to the TE-mode response and the transverse electric field equivalent to the TM-mode response. Accordingly, an east-west strike direction is appropriate for the north-south lines (0, 1, 2, 6, 8), and a north-south strike for the short east-west lines (A, B, C) close to the anomaly.

Performing multisite, multifrequency decompositions of the data from the eight lines in the interpretation frequency band of 1000–30 Hz yields strike directions given in Table 2. With these geoelectric strikes, the data from each line were again decomposed with the adopted geoelectric strike listed in Table 2 and the galvanic distortions removed. Much of the static shift in the levels of the apparent resistivity curves was removed by compensating for site anisotropy, which is the separation of the apparent resistivity curves at the highest frequencies. Correction for anisotropy involves shifting the apparent resistivity curves at each site to the geometric average of the two modes. The remaining unknown amplitude factor, called the site gain by Groom and Bailey (1989), is expected to be small at each site (less than one-quarter of a decade), as demonstrated by analytical modeling studies (Groom and Bailey, 1989, 1991).

The shear and twist values determined for these constrained decompositions are illustrated in Figure 6. As has been observed on other surveys, the shear value shows the largest variation, with a modulus mean of 12.5° and over half in the range 7.5°–15.0°. The twist values have a modulus mean of 6°, with over 65% less than 7.5°. Overall, however, these distortion values are low compared to what is often observed in resistive Precambrian regions.

### Data consistency

As the final preprocessing step, one must ensure that the data are internally consistent prior to 1D or 2D modeling and inversion. One test is the consistency of the observed apparent resistivity estimates with those predicted from the phase estimates using Parker and Booker's (1996) Rho$^+$ algorithm, which is an extension of Parker's (1980) D$^+$ algorithm implemented by Parker and Whaler (1981). Although the Rho$^+$ algorithm was developed for the 1D earth response, it can validly be applied to the 2D TM mode response for any arbitrary 2D conductivity structure (Weidelt and Kaikkonen, 1994). Although no theoretical justification exists, empirically 1D interpretation of 2D TE-mode responses has been studied by a number of authors (e.g., Agarwal et al., 1993), and showed to be possible for all models studied, suggesting a Hilbert transform relationship between the apparent resistivity and phase curves.

Site 005 was chosen to display this procedure. Figure 7 shows the high-frequency decomposed apparent resistivity

data (10 kHz–10 Hz) for site 005 together with the predictions of the apparent resistivities from the phase data. Clearly, the apparent resistivity data in the AMT dead-band range of 3 kHz–800 Hz are inconsistent with the values predicted by the corresponding phases. This confirms the remarks of Garcia and Jones (2002) concerning the poor data typically collected in this band during the daytime.

Figure 8 shows the predicted apparent resistivities based on the phases for the low-frequency response estimates. The observed apparent resistivities at frequencies below 10 Hz drop off far faster than is predicted by the corresponding phase curves. In fact, the rapid decay of the apparent resistivity curves with decreasing frequency to 1 Hz is greater than what is permitted by induction [equidecade decreases for a infinitely conducting substratum (Cagniard, 1953)], shown by the solid lines in the apparent resistivity plots of Figure 8. This rapid decay is independent of the azimuth of the data. Figure 9 shows the logarithm of the apparent resistivities rotated through 90°. This decay cannot be from an inductive process, and we suspect it is due to the galvanic effects caused by alternating surface charges impressed upon the boundaries of conducting discontinuities by impinging currents [Price's (1973) villain of the piece!]. In contrast, the phase is well-behaved at all azimuths (not shown), i.e., it remains within the first quadrant.

The low-frequency apparent resistivity inconsistency was observed at all sites within a particular area defined by sites 005, 007, 004, 003, 402, 401, 608, 616, 607, and 615. From this, we can conclude that the anomalous behavior is not due to instrumental error or a source field problem, but is a local effect only

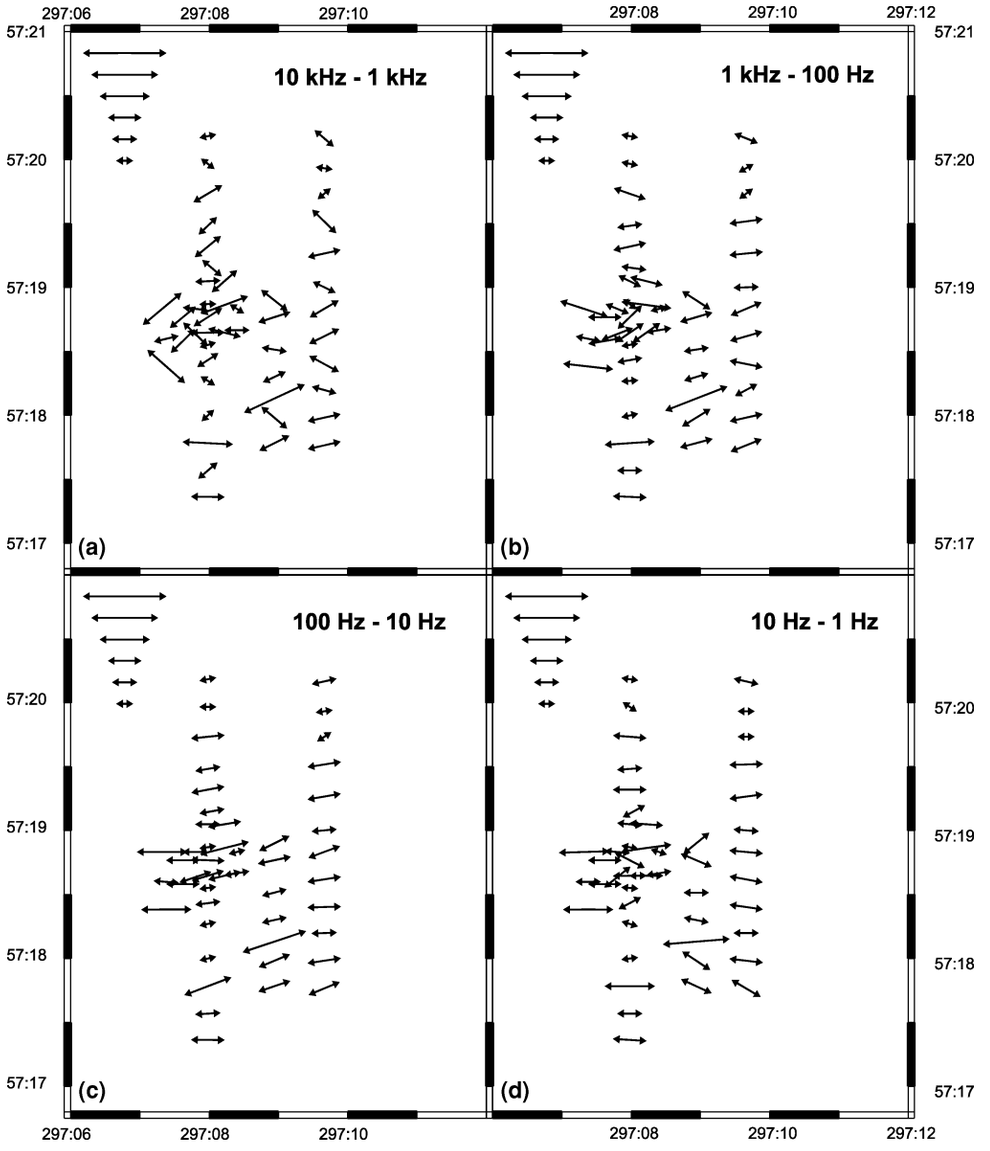


FIG. 5. Maps of the geoelectric strike directions in four decade-wide bands: (a) 10 kHz–1 kHz, (b) 1 kHz–100 Hz, (c) 100–10 Hz, and (d) 10–1 Hz. The length of the arrow indicates goodness of fit, with the longest three arrows having a statistically acceptable misfit and the shortest three arrows having an unacceptable fit.

in the close vicinity of the anomalous body. Our interpretation is that it is caused by galvanic interaction of a conducting body with regional-scale currents.

These consistency checks demonstrate that the parts of the data that can be explained by regional induction lie in the range 1000–10 Hz.

## DATA DISPLAYS

### Decomposed AMT data

Figure 10 shows maps of the tensor decomposed and anisotropy corrected along-strike apparent resistivity ($Z_{xy}$) at four representative frequencies for the sites close to the OK-M1 and OK-M2/M3 drillholes. These frequencies are sensing depths (based on skin depth arguments) of approximately 400–800 m, 800–2000 m, 2000–4000 m, and 4000–8000 m, respectively. They should be interpreted with care, as they are not true images of the resistivity of the subsurface but representations of the resistivity filtered through spatial averages, both in distance and in depth.

The maps present a self-consistent image of the region around the drillholes. At the highest frequency of 768 Hz (Figure 10a), a region of enhanced conductivity is sensed in the vicinity of the triangle formed by sites 004, 007, and 003. This implies that there is a body at a depth of around 500 m in this location, which is consistent with the intersection depth of 450 m for OK-M3. Also, the center of the resistivity low, lying in the triangle formed by sites 004, 007, and 003, is consistent with the reported westward thickening of the mineralization from 70 m in OK-M1 (489.2–558.2 m) to 151 m (vertical) in OK-M2 (544.0–701.9 m at 73.5°) and 120 m (vertical) in OK-M3 (496.4–569.7 m and 589.6–636.8 m at 85°).

The maps illustrate that there are no other strong zones of interconnected conductivity in the region. The only anomaly is in the vicinity of the existing drillholes.

Figures 11 and 12 display pseudosections of the distortion-corrected and shift-corrected apparent resistivities (Figure 11)

**Table 2. Preferred geoelectric strike angle determined for each line in the frequency band 1000–30 Hz.**

| Line (number of sites) | Strike (in degrees) |
|---|---|
| 0 (7) | 90 |
| 1 (7) | 73 |
| 2 (12) | 80 |
| 6 (17) | 83 |
| 8 (3) | 75 |
| A (8) | 0 |
| B (8) | −17 |
| C (4) | −15 |

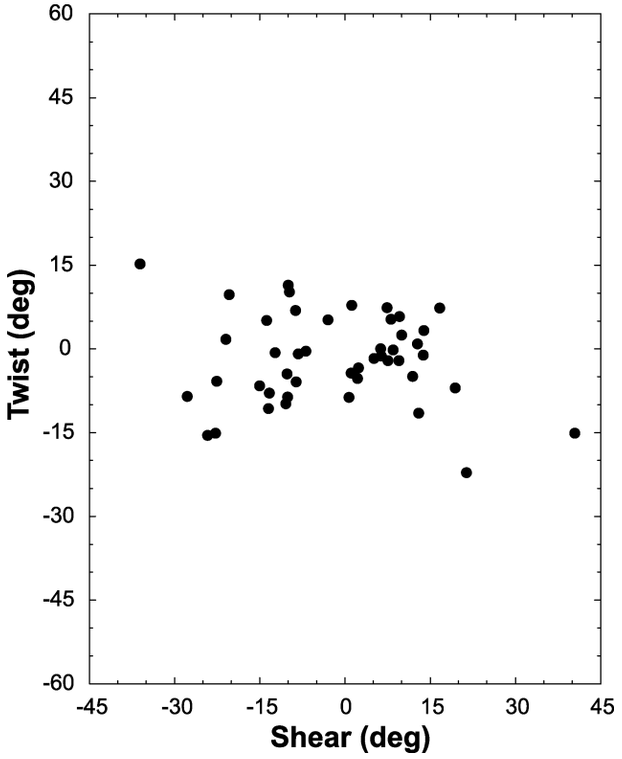


FIG. 6. Frequency-independent shear and twist estimates in the frequency range 1000–30 Hz for all 46 sites with the strike directions constrained to those listed in Table 2.

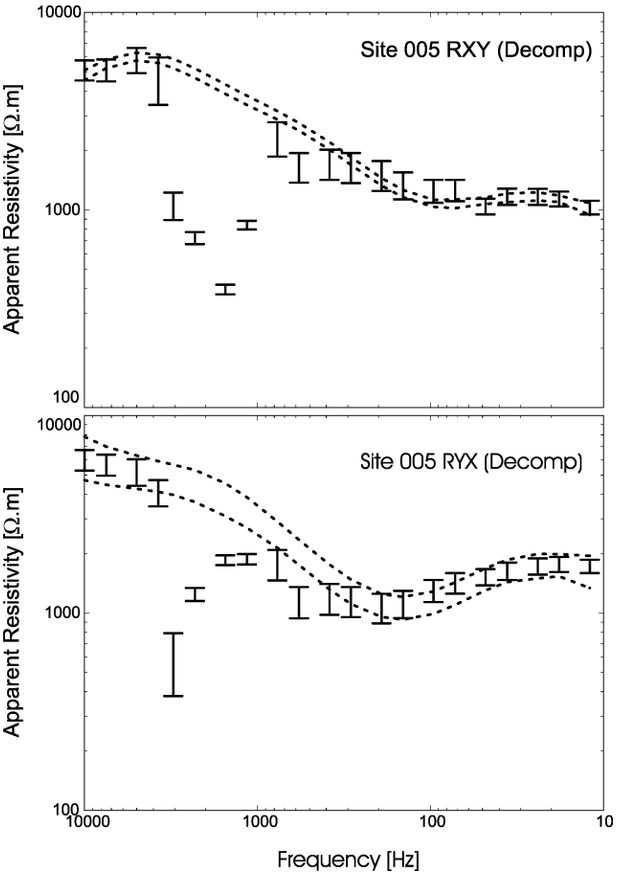


FIG. 7. Derived high-frequency tensor decomposed apparent-resistivity data for site 005 together with their prediction (dashed lines show ± one standard error) from the phase data using Parker and Booker's (1996) Rho$^+$ algorithm.

and phases (Figure 12) from line 6. There is a strong anomaly in the TE pseudosection (Figure 11, top) at sites 615, 607, 616, and 608, particularly at frequencies below 10 Hz. This low-frequency response is discussed above. The TM apparent resistivity (RhoTM) pseudosection (Figure 11, bottom) shows a general reduction of resistivities in this region. The phase pseudosections do not show a strong high phase anomaly as would be expected from the model depicted in Figure 3.

## Induction vectors

The geomagnetic transfer function between the vertical magnetic field component and the horizontal magnetic field components can be expressed asreal and imaginary induction vectors, and the real vector, when reversed, usually points towards regions of enhanced conductivity (Jones, 1986). Over a 1D earth, and also directly on top of a symmetric 3D anomaly, there is no induced vertical magnetic field. Accordingly, an observed vertical magnetic field implies that there must be lateral variations in electrical conductivity within an inductive scale length of the station. These vectors have been used qualitatively in regional studies to map areas and find anomalies, and were first used in Australia where they pointed towards electrical current concentration at the coastlines (Parkinson, 1962).

Maps of these vectors illustrate that there are problems with the geomagnetic transfer function estimates for these data. The vectors are generally inconsistent both in length and azimuth from site-to-site and, accordingly, a quantitative interpretation is not possible. There is very poor data quality, particularly in the AMT dead-band centered on 1536 Hz. This is unfortunate as theoretical tests demonstrate that for a body at depths of 500–700 m (i.e., the depth of mineralization intersected by the drillholes), the maximum geomagnetic transfer function response is in the frequency band 3000–1000 Hz.

A map of the induction vectors at 768 Hz for the sites closest to the drillholes (Figure 13a) shows, as expected, very small vectors for sites on or close to the anomaly (sites 004, 007, 003, 401), with others nearby generally pointing towards them. Sites 616, 402, 803, and 609 have questionable vectors, suggestive of layout or calibration errors.

At low frequencies, beginning at 96 Hz, the real vectors all point northeast towards Okak Bay. Although the nearest ocean water is over 25 km away in Okak Bay, and the Atlantic coastline is almost 50 km away, the electric currents concentrated at the ocean-land boundary can be sensed at frequencies as high as tens of Hertz. Even for the high crustal resistivities in the region, the coast is many skin depths away from the anomaly,

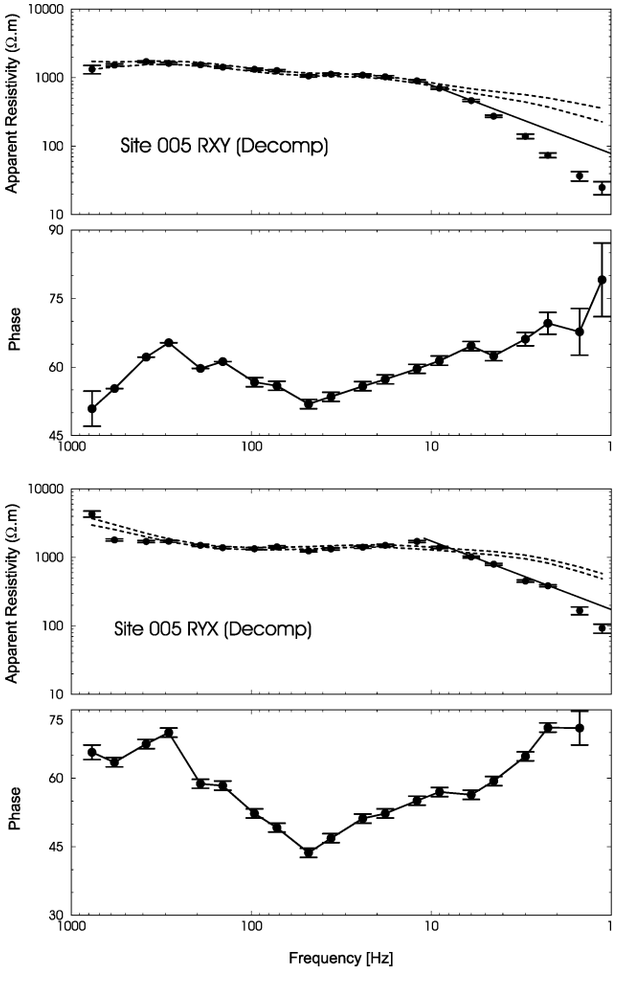


FIG. 8. Derived low-frequency tensor decomposed apparent-resistivity data for site 005 together with their prediction (dashed lines show ± one standard error) from the phase data using Parker and Booker's (1996) Rho$^+$ algorithm. The solid lines in the apparent resistivity plots show the decay for an infinitely conducting substratum. Also shown are the decomposed phase data.

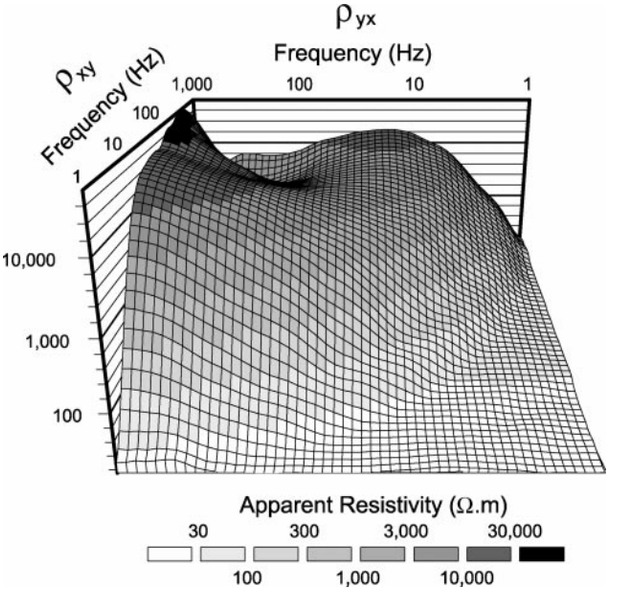


FIG. 9. Rotation of the apparent resistivity data in the frequency range 1000–1 Hz from site 005 with azimuith from 0° ($\rho_{xy}$) to 90° ($\rho_{yx}$).

and so one might not intuitively expect this result. However, as discussed by Ranganayaki and Madden (1980), Dawson et al. (1982), and Jones (1983), the appropriate scale length is given by the adjustment distance, not the skin depth, and at low frequencies this distance can be many hundreds of kilometers. As formulated by Ranganayaki and Madden (1980) and Dawson et al. (1982), this distance applies on the ocean side of the coastline, so it cannot be directly applied as there is no conducting upper thin sheet on the land side. Nevertheless, the induction arrows clearly indicate that there is an observable effect.

Forward modeling studies show that if there is a conducting anomaly at 1–3 km, as depicted in Figure 3, this anomaly would have its maximum geomagnetic transfer function response at approximately 10 Hz. A map of vectors at 12 Hz (Figure 13b) shows only the distant coast, and no response to any extensive deep conducting bodies. (The vectors at sites 401 and 615 are anomalously small and the geomagnetic transfer function is close to zero at all frequencies, suggesting a problem with acquisition of the vertical magnetic field component at these sites.)

## 1D INVERSIONS

The high-frequency (>100 Hz) parts of the data set respond in an almost 1D manner, i.e., the apparent resistivity and phase curves of the two modes (TE and TM) overlie one another. Thus we can use 1D MT tools to investigate the shallow structure beneath important sites. We have chosen sites 004 and 005 for presentation; 004 is closest to the holes drilled on the basis

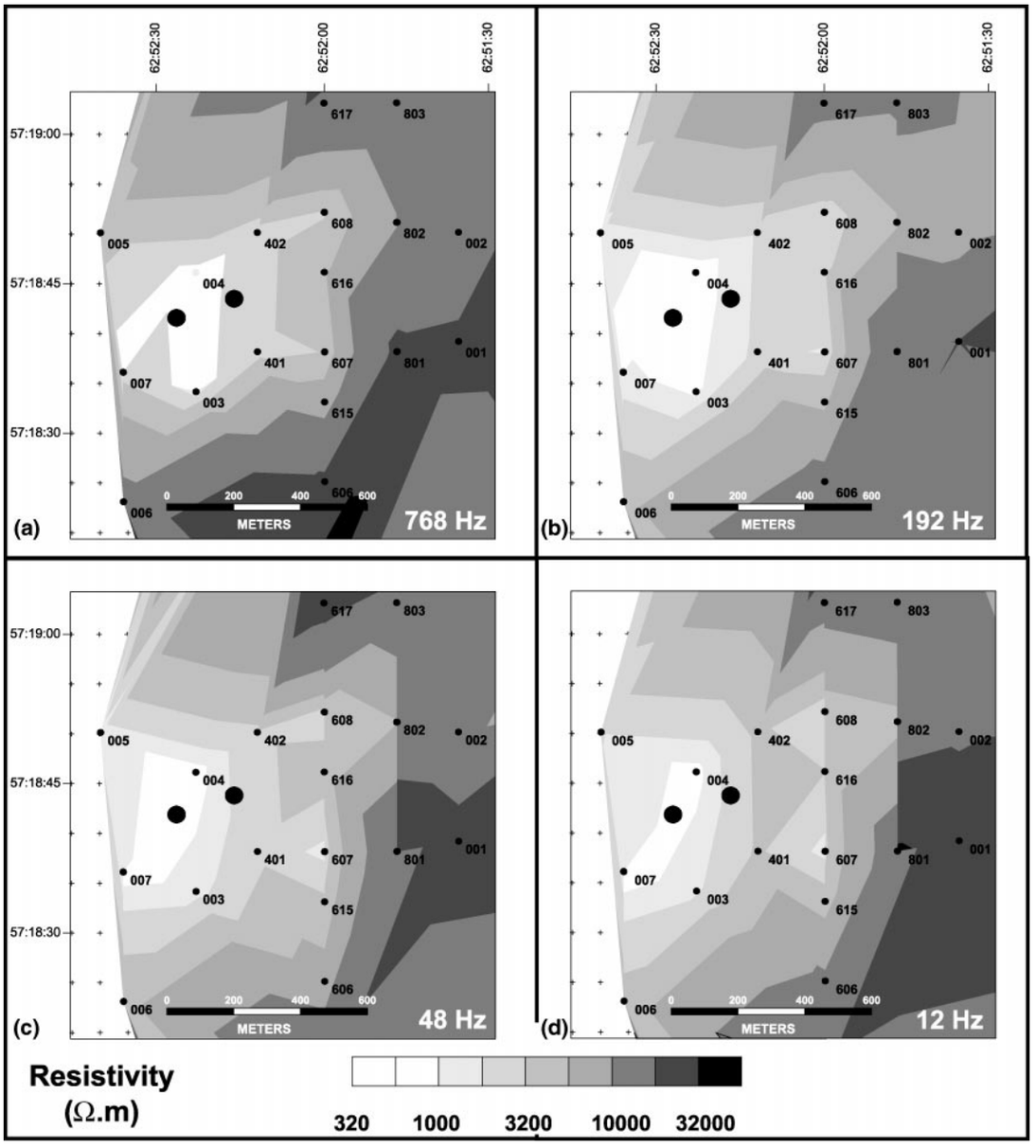


FIG. 10. Maps of distortion-corrected averaged apparent resistivities at four frequencies: (a) 768 Hz, (b) 192 Hz, (c) 48 Hz, and (d) 12 Hz.

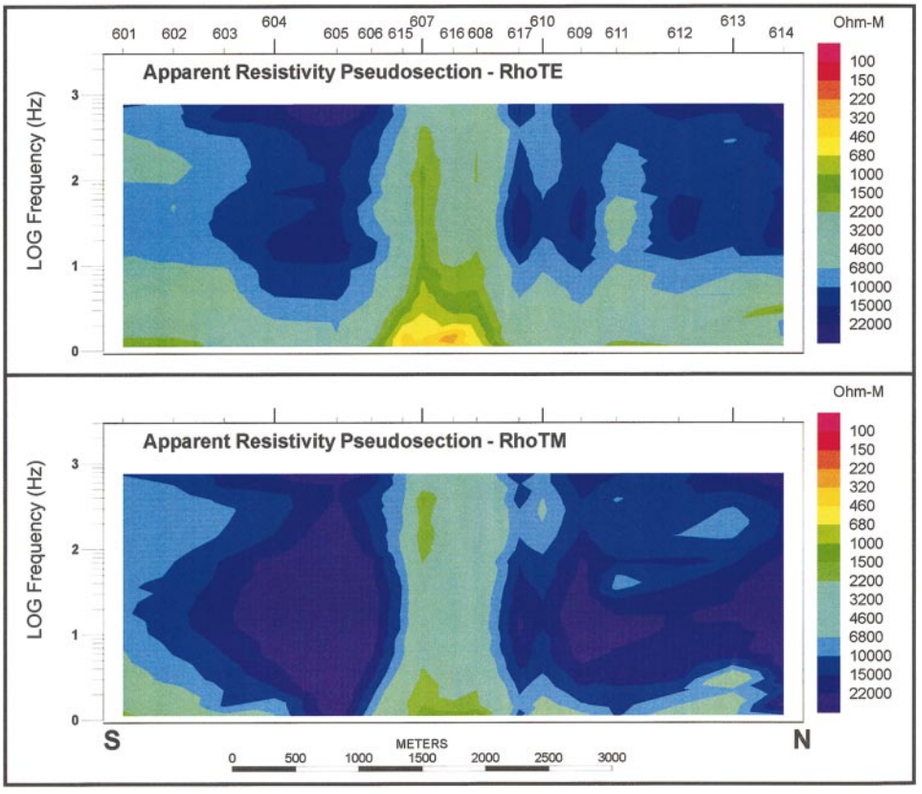


FIG. 11. Apparent resistivity peudosections of the distortion-corrected data from line 6.

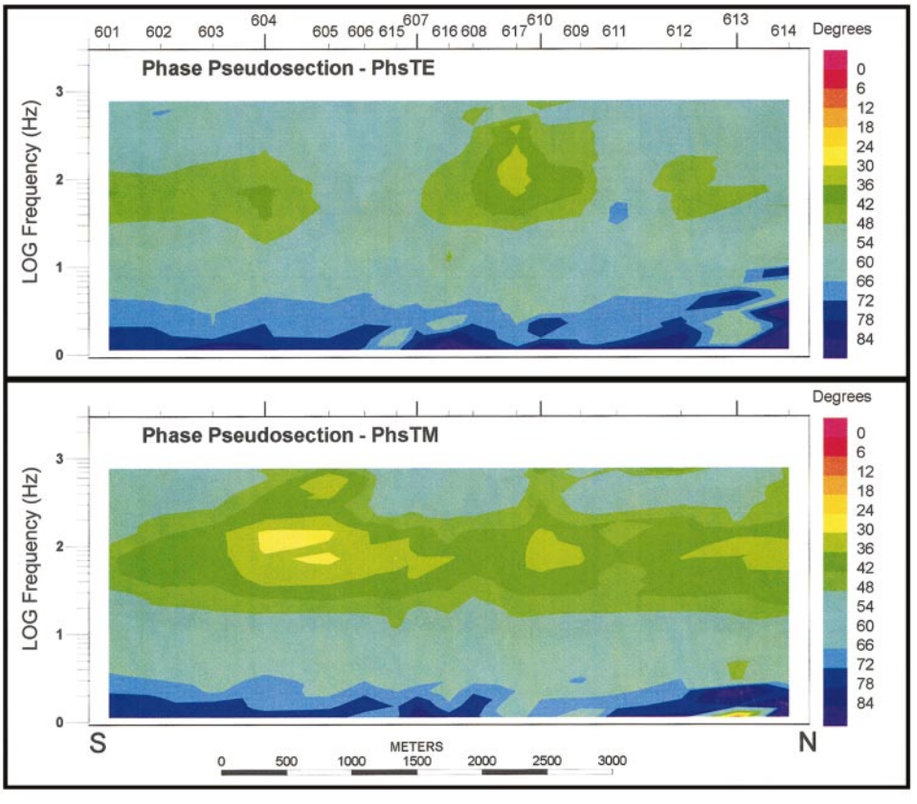


FIG. 12. Phase peudosections of the distortion-corrected data from line 6.

of the AMT results (OK-M1, OK-M2, and OK-M3) and 005 is at the center of an anomaly observed in data from the TEM survey.

### Site 004

A detailed examination of the data from site 004 was undertaken in order to extract as much information as possible given the site's location closest to the three holes drilled that intersected mineralization: OK-M1, OK-M2/OK-M3 (Figure 2). An inversion to obtain the best-fitting model, which comprises conductance "spikes" ($D^+$, Parker and Whaler, 1981), of the decomposed and anisotropy-corrected data, with the TE-mode (ZXY) data directed N80° E and the TM-mode (ZYX) data directed N10° W, gave conductance spikes above 1 km at the depths listed in Table 3. The information from the two orthogonal directions is consistent with an anomaly of about 1.5–S total vertically integrated conductance centered at a depth of around 500 m.

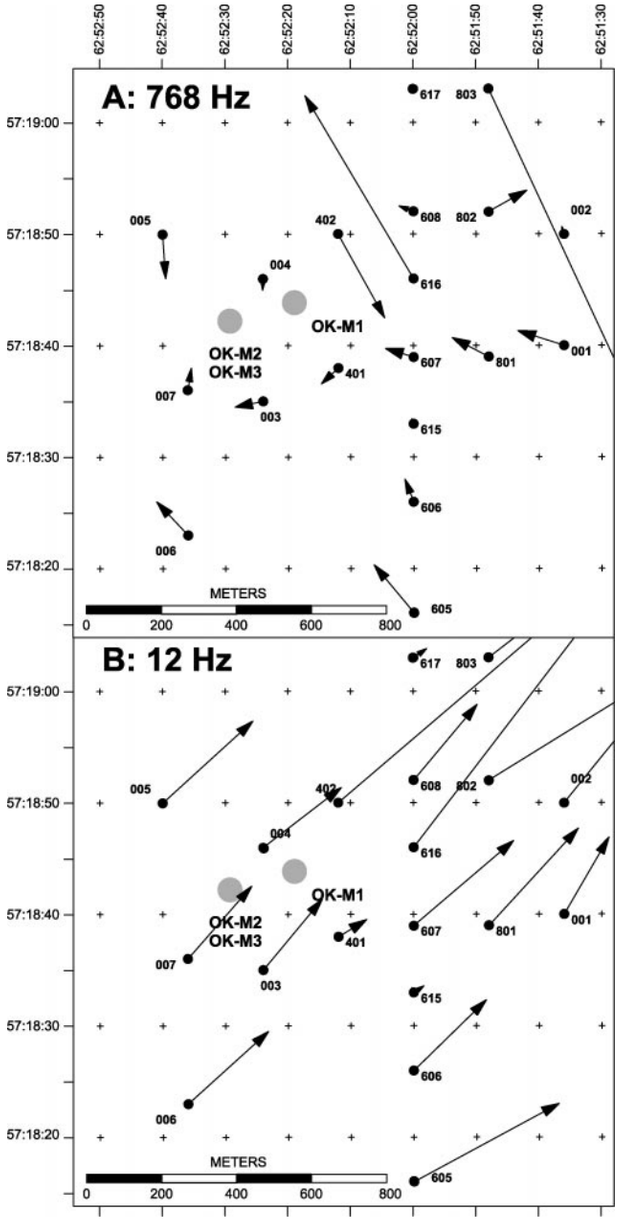


FIG. 13. Reversed real induction arrows at (a) 768 Hz and (b) 12 Hz.

One-dimensional layered-Earth inversions (Fischer and Le Quang, 1981) of the TE- and TM-mode data and of the arithmetic average of the two modes gave the model parameters for the uppermost kilometer listed in Table 4. Singular value decomposition (SVD; Edwards et al., 1981; Jones, 1982) sensitivity analysis of the averaged response model (ZAV) shows that the parameters of the top of the conducting layer are reasonably well-resolved, with a standard error for the depth to the conducting zone of 450–600 m, and a standard error for the conductance of the conducting zone of 1.85–2.15 S. The top of the layer correlates well with the zone at 454 m depth in drillhole OK-M3.

The electrical conductivity of magnetite can range from $10^5$ to $10^{-5}$ S/m, with an average value of $10^4$–$10^3$ S/m, depending on the interconnectivity. Pyrrhotite has a smaller range, from $10^6$ to $10^3$ S/m, with an average of $10^5$–$10^4$ S/m. Assuming that the 2-S conducting zone is primarily due to the pyrrhotite in the 16.4-m depth interval between 454.1 and 470.5 m, reported to be up to 10% disseminated sulfides, then the layer has an averaged interval resistivity of 8.2 ohm-m (16.4 m/2 S). For a nominal mineral conductivity of $10^4$ S/m then, by Archie's Law with an exponent of two, the averaged interconnected pyrrhotite content required to explain the 2-S conductance is approximately 0.3%. Alternative assumptions about the topology of the interconnectivity can be made, with the modified brick layer (MBL) model of Schilling et al. (1997) being perhaps the most general. The MBL model also suggests a conductive fraction of around 0.3%. However, both Archie's Law and the MBL model, as well as others discussed in Jones (1992), describe interconnectivity for ionic conduction in porous media. Whether these models are also appropriate for electronic conduction in dry rocks has yet to be established.

### Site 005

The AMT responses from site 005 exhibit problems in the range 3 kHz–1 kHz, as noted above and shown in Figure 7. The phases look reasonable in this range, but the apparent resistivity estimates are scattered and downward-biased, and are unusable. The highest frequency XY phases show a decay, or droop, towards 0° (Figure 14). The contractor noted very

**Table 3. Conductance spikes above 1 km obtained using Parker and Whaler's (1981) $D^+$ algorithm for the corrected responses from site 004.**

| ZXY (=TE mode) | | ZYX (=TM mode) | |
|---|---|---|---|
| Depth (m) | Conductance (S) | Depth (m) | Conductance (S) |
| 277 | 0.19 | 0 | 0.11 |
| 473 | 1.32 | 513 | 2.04 |

high dc levels for the north-south electrode array (82 mV), which may indicate electrode deterioration. This would result in capacitive coupling to the ground that manifests itself as a low-pass RC-like filter. Alternatively, it may indicate a spontaneous polarization (SP) effect from the shallow anomaly mapped, but the lack of a corresponding droop on the other component (PhsYX) supports the conclusion of an electrode effect.

The lack of high-quality data in the band 3 kHz–600 Hz is most unfortunate because this is exactly the frequency range that would be sensitive to an anomaly at depths of approximately 100–200 m initially thought to be responsible for the observed TEM anomaly. A 16-m-thick layer of 10 ohm-m at a depth of 100 m would have an AMT response as shown in Figure 14, and is compared to the observed data also shown in the figure. There is poor correspondence between the model and the data, particularly with the shape of the phase curves. This lack of correspondence in the AMT data is counter to the interpretation of the TEM data of the existence of a layer of conductance of 2 S at a depth of 100 m below site 005. A weak conducting zone is imaged at around 450 m when the data are fit by a smooth 1D model algorithm (OCCAM models, Constable et al., 1987), and layered earth inversion (Fischer and Le Quang, 1981) suggests a 0.6-S conductor at a depth in the interval 450–550 m (451 m TM; 505 m AV; 540 m TE), but this depth is weakly constrained, with a standard error of 120 m due to the poor data quality. Drilling in September 1999 in the center of a TEM anomaly (hole OK-M8, close to site 005) intersected a 3.5-m-thick zone of mineralization at a depth of 523.6 m, consistent with this weak conductor. Although the mineralization intersected by the borehole has high concentrations (locally up to 50% disseminated sulfide mineralization), the weak AMT response seen at site 005 suggests that it is either of limited extent or is poorly interconnected electrically.

In conclusion, although the AMT data are inconsistent and unusable in the 3 kHz–1 kHz frequency band most sensitive to the presence of an anomaly initially thought to explain the observed TEM response, it is possible to exclude the existence of a 2-S mineralized zone at 100–200 m depth. The anomaly required to explain the usable AMT data is one of 0.6 S at a depth of 450–500 m, and the AMT response most sensitive to it is the phase maximum at 300–400 Hz (Figure 14). This AMT frequency compares well with a TEM maximum anomaly time channel of 0.55 ms, which converts to approximately 360 Hz.

## 2D INVERSIONS

The distortion-decomposed data on the nine profiles were inverted using the *rund2inv_nlcg2* 2D inversion code of Rodi and Mackie (2001). The inversions were performed using the data in the 1000–10 Hz frequency range, with a minimum error floor of 3.5% in the apparent resistivities and 1° for the phases (i.e., if the estimated errors were less than these floor values, they were set to these values). The starting model in each case was a uniform half-space of 1000 ohm-m. The final misfits of both mode inversions for all models are relatively small [normalized root mean square (rms) around 6, but with a good visual fit to the character of the data]. Better fits are achieved for the TE- and TM-mode data separately, suggesting either the presence of spatially aliased local site-to-site variation or off-profile 3D effects, or both.

### Validity of 2D inversion of 3D structures

As discussed by Jones (1983), in situations where the earth is 3D, then a valid 2D interpretation may be undertaken of the TM-mode data when the end of the 3D anomaly is greater than 0.1 skin depths in the host medium. For a host medium of 5000 ohm-m, and a distance to the "face" of 580 m, then the TM inversion is valid to frequencies as low as 35 Hz. At lower frequencies, the off-profile 3D body will affect the resulting model. However, for the TE mode, the effects of an off-profile body are seen at much higher frequencies. The approximate rule-of-thumb is that the TE-mode data are affected by bodies lying off-profile within one skin depth. Wannamaker et al. (1984) also concluded that 2D TM inversion of data over a 3D body is likely to produce the most accurate result. However, Park and Mackie (1997) show that for some geometries it is the 2D TE-mode data that are closest to the 3D response.

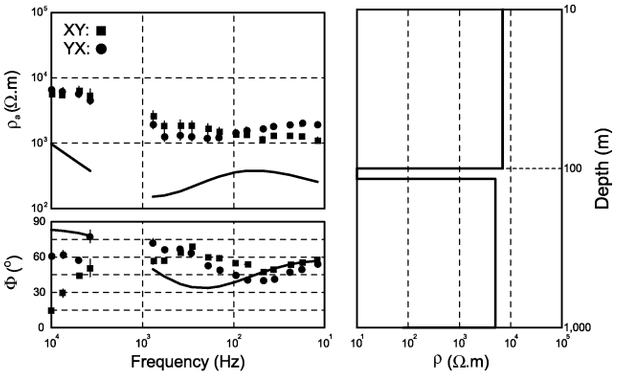


FIG. 14. Distortion-corrected data from site 005 compared to a 1D model which includes a conducting layer at 100 m with the same conductance as observed in drillhole OK-M3 in the interval 454–470 m.

**Table 4. One-dimensional layered earth parameters of the top kilometer for the corrected responses from site 004 (Rho = layer resistivity in ohm-meters; H = layer thickness in meters).**

| | ZXY (=TE mode) | | ZYX (=TM mode) | | ZAV | |
|---|---|---|---|---|---|---|
| Layer | Rho | H | Rho | H | Rho | H |
| 1 | 3700 | 445 | 1878 | 496 | 1753 | 520 |
| 2 | 53 | 75 | 54 | 98 | 50 | 100 |
| 3 | 1940 | | 10500 | | 3845 | |

Martinelli et al. (2000) undertook a comparison of 2D inversion of 3D data for a problem with an embedded inhomogeneity, and showed that whereas the geometry of the top and sides of the body is reasonably well-recovered, the 2D models underestimated the thickness of the conductor by up to 30% (i.e., underestimate the total conductance by that amount). The TM-mode equivalent model is closest to the true cross-section of the 3D model, but the TE-mode equivalent model is also a reasonable approximation to that cross-section. This study suggests that joint inversion of TE- and TM-mode data together will result in a model with a conductance of the embedded inhomogeneity that is in error by at most 50%, and more likely less than 25%.

### Tests of preliminary model

To test the resolving properties of the inversion code used, the preliminary model of Figure 3 was simplified and parameterized (Figure 15a), and its theoretical forward response calculated at the same sites and same frequencies as the actual data. As well as the deeper anomalies, shallow ones were included beneath sites 604 and 616 (100-m depth) and surficial anomalies beneath sites 609, 613, and 614. There is little TM response to the structures, and the maximum TE response to the large central deep (1–3 km) conductor is in the frequency band of 100–10 Hz for apparent resistivity and 100–1 Hz for phase.

We inverted the synthetic data for this model data at 13 frequencies in the range 1000–10 Hz, with an assumed error of 3.5% in apparent resistivity and 1° in phase. The starting model was a uniform 1000-ohm-m half-space. The final model, with a normalized rms misfit of one (i.e., the data were fit to the level of the error bars) and obtained after 82 iterations, is shown in Figure 15b. All the anomalies in the model are "discovered" when inverting the data. The shape of the main anomaly is poorly resolved, which is due to the well-known difficulty in resolving the base of conductors with EM methods.

The model illustrated in Figure 15c is that obtained from inverting the TM-mode data alone. The model was found after

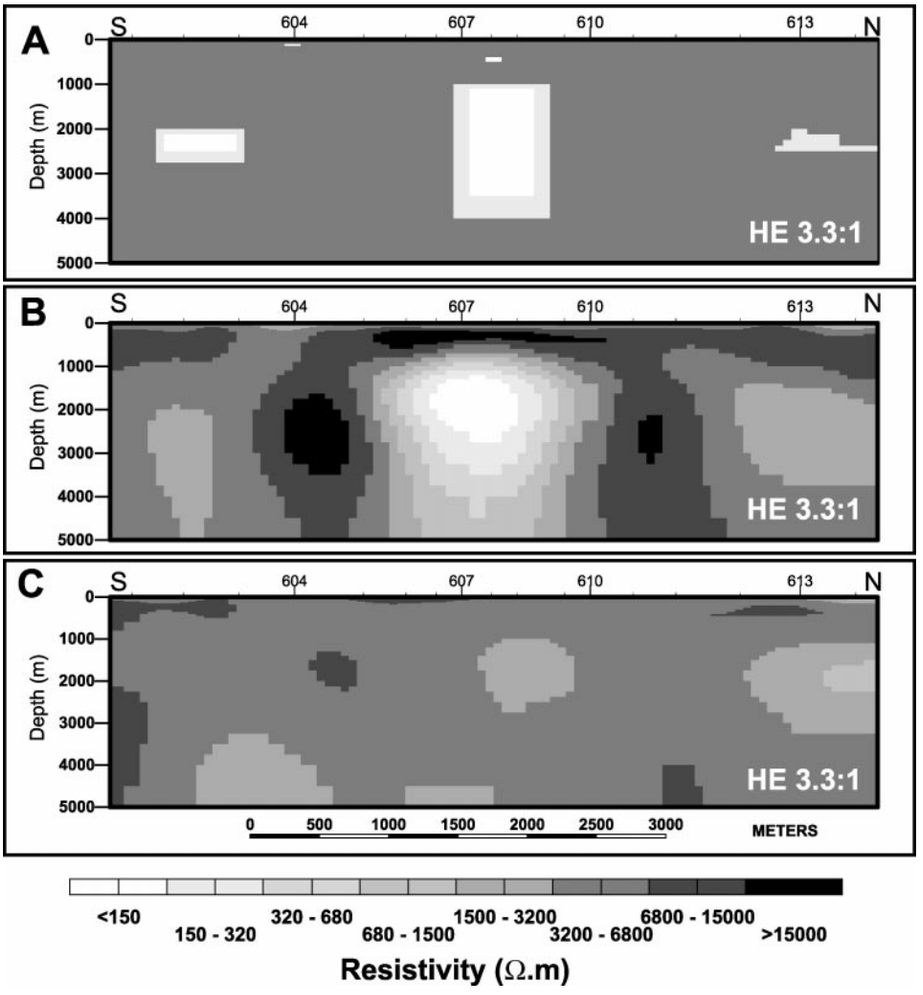


FIG. 15. (a) Test model based on the preliminary model (Figure 3), and inversion of (b) both modes and (c) TM-only mode, of the synthetic MT data in the range 1000–10 Hz. (Note the horizontal exaggeration of 3.3:1.)

37 iterations, with a smaller misfit of normalized rms = 0.5. This model only shows a very weak image of the large conductor, demonstrating the well-known problem with TM data for imaging "thin" subvertical anomalies (see discussion below). The spurious conductor to the north of site 613 is an edge artifact of the inversion code.

### Line 6

**Joint TE and TM inversion of the distortion-corrected line 600 data.—**The final model obtained by jointly inverting the distortion-corrected TE- and TM-mode data simultaneously is shown in Figure 16a. This model has an rms misfit of 3.5; thus, it does not fit the data to within the set statistical tolerances. The TM-mode data (RhoYX and PhaYX) are fit reasonably well, and most of the misfit is in the the TE-mode data (RhoXY and PhaXY). We attribute this problem to incompatibility of the TE with the TM data, and interpret this as due to off-profile structure appearing in the TE-mode data, but not in the TM-mode data.

The only anomaly found is between sites 607 and 608 at depths of some hundreds of meters with an apparent dip to the south. There is no evidence of the deeper conducting feature in the contractor's preliminary model (Figure 3).

**TM-only inversion of the distortion-corrected line 600 data.—**It should be noted that although TM data have the advantage that they are less sensitive to off-profile structures, they have the distinct disadvantage that they are also insensitive to certain classes of anomalous structures. These structures are ones in which the anomaly (or anomalies) is (are) thin in a lateral sense (Jones, 1993; Jones et al., 1993). This is a serious restriction for mineral exploration studies, where the enhanced conductivity often lies along thin zones (Jones et al., 1997). The final TM model found is shown in Figure 16b. This model does bear some resemblance to the test TM inversion of the model shown in Figure 3, demonstrating the poor sensitivity of TM data to the presence of vertical conducting anomalies.

### Line 0

Profile 0 is the westernmost profile in the data set (Figure 2), and is located on top of the aeromagnetic anomaly. The data

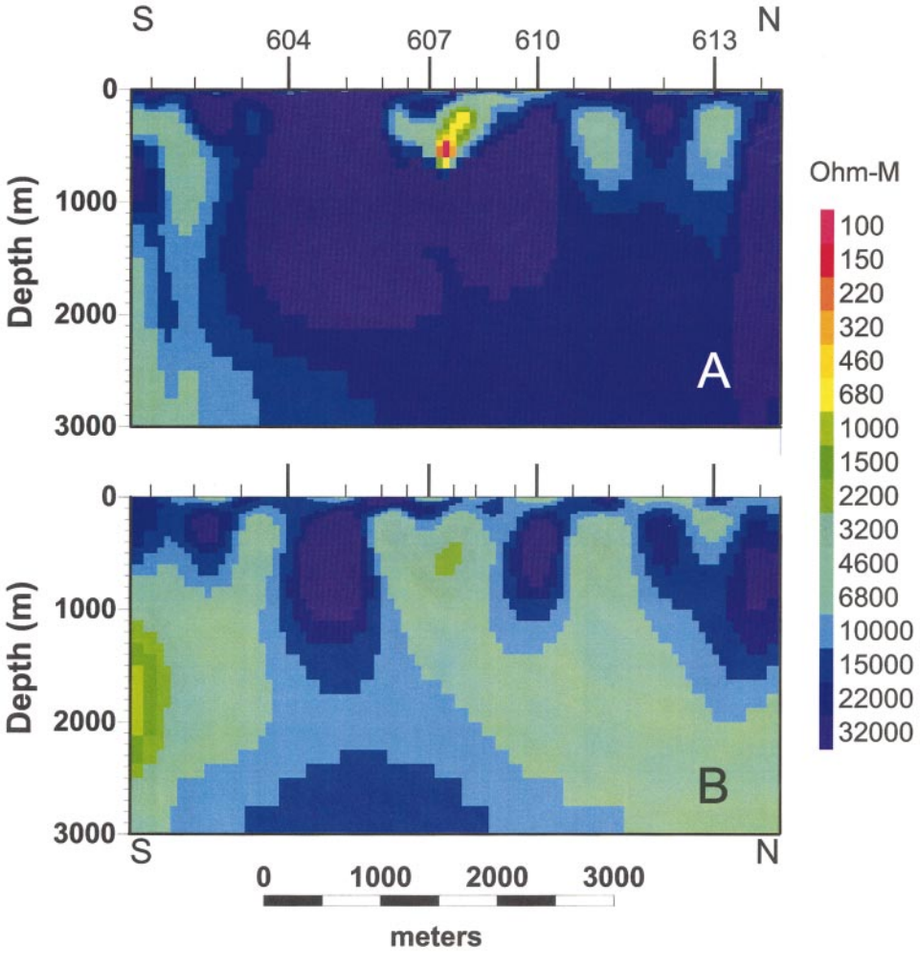


FIG. 16. (a) Inversion of both modes of data for the line 6 sites. (b) Inversion of TM-mode only data for the line 6 sites.

are subject to strong 3D effects due to the presence of small conductors. The fact that the mineralized zone is located to the east of the profile may be the cause of the difficulty in inverting both modes simultaneously.

For the inversion, we started with simultaneous TE- and TM-mode inversions, then used the best model obtained as the starting model for a new inversion until the misfit could not be improved. Subsequently, a new set of iterations was performed using either TE or TM data alone. The final model for both modes of inversion (Figure 17) does not differ significantly from the models obtained from single mode inversions. The fit of the model to the data is very good for the single mode inversions but is poorer using both modes.

### Line 8

The final model obtained for the data from Line 8 (Figure 17) shows the presence of a conductor at approximately 200-m depth located under station 802. The body is 200-m long and 100-m thick, with a resistivity of around 50 ohm-m, for a total integrated conductance of 2 S. The model fits the data with a final normalized rms of 3.2, and the misfit is mostly in the TE mode, which again we take as indicative of 3D effects due to an off-line conductor.

### Lines 1 and 2

Lines 1 and 2 are located outside the area of interest. The final model for line 1 (Figure 17) does not reveal any conductive structures with resistivity below 1000 ohm-m. The fit to these data is very good, with a few stations that show very local 3D effects that could not be removed by the decomposition procedure.

The line 2 data are similar to those from line 1. The final model (Figure 17) does not indicate the presence of any conductive structures with resistivity below 1000 ohm-m. The fit is very good, and only station 201 is anomalous, probably due to noise in the data.

### Line A

Line A is the northernmost east-west profile. The first inversions were performed using eight stations (005, 004, 402, 608, 802, 002, 106, and 207). Due to the presence of the mineralized zone in the western part of the profile, it was not possible to obtain a 2D model for the whole profile. The profile was shortened by dropping the easternmost sites, and it extends from station 005 to station 802. Station 005 shows an anomalous apparent resistivity and, in order to fit the data, the error bars corresponding to the highest frequencies were increased by a factor of two to allow a fit of the phase that is more consistent with the neighboring stations.

The model (Figure 17) shows a conductor below stations 005 and 004 dipping to the west. This conductor is more than 300-m long, 100-m thick, and presents an anomalous region of resistivity between 50 and 10 ohm-m in its eastern part, decreasing to 1 ohm-m at its western termination. As station 004 is off the profile line, this conductor is due to the lateral effects of the conductors located south of the profile. The fit is not very good, but the model reproduces the behavior of the data.

### Line B

Line B presents the same problems as line A. The lack of sufficient spatial coverage to study the anomaly, the noisy

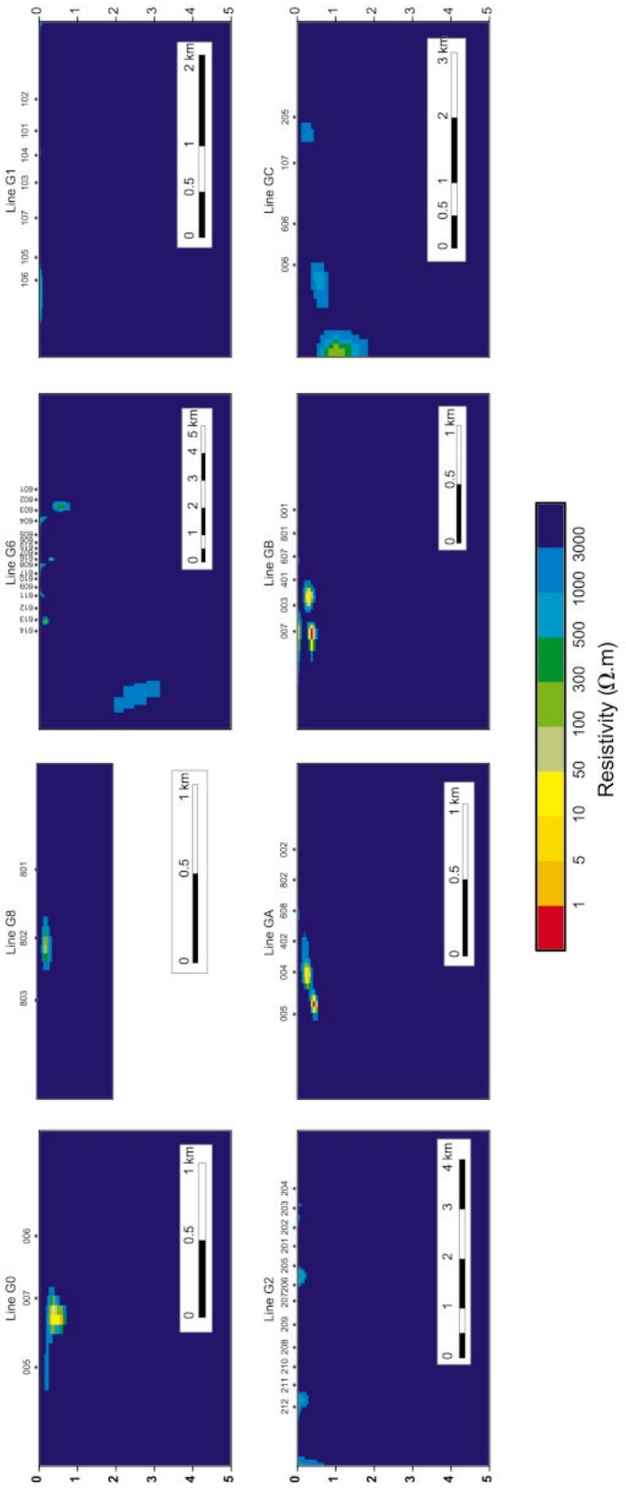


FIG. 17. Inversions of the data from all lines.

responses, and the clear 3D nature of the data seriously complicates the inversion of the data from this profile.

The model (Figure 17) shows two conductive structures that correlate with the structure found in line 1. The conductive structure located below stations 003 and 401 is the conductor intercepted by the drill holes in that area (OK-M1, OK-M2, and OK-M3). Under station 007 there is a second conductor, of reduced dimensions, that is equally traced by the inversion of the line 0. There is a large misfit of this model to the data, especially in the TE mode.

### Line C

Line C is the southernmost east-west profile. The model obtained (Figure 17) does not show the presence of any conductive structures in the area. The fit to the data is very good at all frequencies.

### Line Z

The northwest-southeast line Z was constructed in an attempt to determine better the geometry and resistivity value of the conductor traced by the drillholes. The stations that form this profile are 005, 004, 401, and 615. The MJ decomposition of the data along this profile suggested that the best strike to represent this data in a 2D fashion is 80° (N80° E).

The model obtained for this profile is shown in Figure 18. It shows a large conductor below station 004, slightly dipping to the northwest. This conductor is approximately 800-m long and 200-m thick at a depth of approximately 400 m. This is the conductor intersected by the drillholes in the area (OK-M1, OK-M2, and OK-M3) and comprises the pyrrhotite in the 16.4-m depth interval of 454.1–470.5 m. The fit of the data is good for the TM mode, but less satisfactory for the TE mode, particularly at stations 005 and 615. This profile intersects line B at station 401 and shows good agreement between both models in the vicinity of the conductive area.

## 3D IMAGING AND MODELING

### Pseudo-3D model

In order to obtain an approximate geometry of the conducting body, we have constructed a pseudo-3D model using all the 2D models that cross, or are close to, the target body (A, B, C, Z, 0, and 6). This model is a block with corners predominantly defined by stations 005, 608, 606, and 006. It should be noted that the 2D inversion code places smooth edges on anomalous structures, so conductors will have lower bulk conductivity and larger dimensions than may be correct. Also, 2D models place lateral conductors directly beneath the profile, which may result in false images of the conductive structure due to off-line effects. Finally, to construct this structure we had to interpolate between profiles. Accordingly, this model should be interpreted in a qualitative sense only.

Figure 19 shows four slices through the pseudo-3D model with a transparency filter for resistivities over 50 ohm-m applied. The isosurface determined by resistivity below 50 ohm-m is shown in Figure 20; this represents the conductivity structure alone. The position of this conductive structure correlates well spatially with the conductive mineralized zone found through drilling.

The pseudo-3D models locate the conductive structure at a depth of 500 m with a resistivity of <50 ohm-m, and is located in the square formed by stations 005, 004, 003, and 007. This body was intersected by the drillholes in the area (OK-M1, OK-M2, and OK-M3).

The forward response of a stylized body with the approximate dimensions and geometry was computed using the extended Born algorithm of Habashy et al. (1993), as implemented in the EMIGMA code of PetrosEikon. In the frequency range of our interpretation (1000–30 Hz), the observed responses were qualitatively explained by the body.

### 3D regional model

As pointed out above with regard to low-frequency data inconsistency and induction vector response, some of the

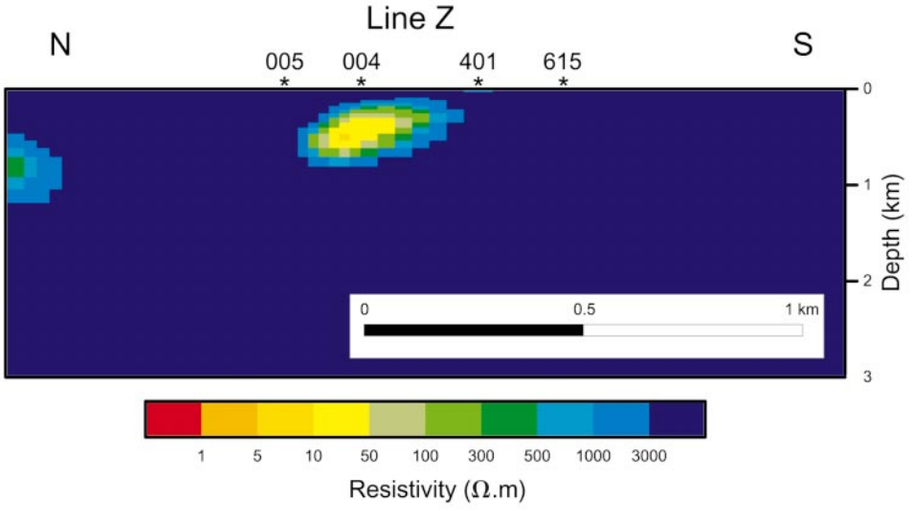


FIG. 18. Inversion of the data from line Z over the top of the drillholes.

difficulties in understanding the data in a 2D fashion arise from the proximity of the ocean to the study area. The induced currents in the ocean couple inductively and galvanically with the conductive structure, and the effects manifest themselves as an apparent enhancement of the anomaly's conductivity and its lateral and vertical extent. Possibly other noneconomic (graphitic) conductors between the anomaly and the coast contribute to this coupling effect by channeling regional current flow through the area. Detailed maps by Ermanovics et al. (1997) and Ermanovics and van Kranendonk (1998) show outcrops of black shale units and metasedimentary units that contain locally massive (up to 15-cm thick and several meters long) pyrite veins. Such an effect was previously reported by Livelybrooks et al. (1996), who observed an EM response of the Trillabelle deposit that was in excess of expectations based on 3D modeling of the body.

To understand the effect of the Atlantic Ocean and Okak Bay, 3D forward modeling was undertaken with a conductor representative of the target body in the study area (resistivity 1 ohm-m) within a homogeneous half-space of 10 000 ohm-m, and modeling the ocean 50 km to the east (Figure 21). This type of 3D model with a range of scales from tens of meters to hundreds of kilometers is difficult to compute numerically using conventional approaches. Accordingly, we used the extended Born algorithm of Habashy et al. (1993). We calculated the forward response of three models. The first model contains both the target body and the ocean. The second model has only the target body without an ocean (discussed above), and the third model has only the ocean.

We were unable to reproduce the fundamental curious observation, which is of a significant effect on apparent resistivity data below 10 Hz with little corresponding effect on the phase curves at those sites in the closevicinity of the anomaly (Figure 8). In contrast, the 3D modeling showed a large phase effect due to interaction between the body and the ocean currents for one mode of induction. The phase pseudosections correspondent to all these models are shown in Figures 22 (XY mode, with X = east and Y = north; electric currents traveling east-west, i.e., crossing the coastline) and 23 (YX mode; electric currents traveling north-south, i.e., along the coastline). As can be observed, the effect of the ocean is apparent in the data, manifest under the profile as an apparent conductive layer that is just the electrical image of the ocean. What is more significant is that for those sites on top of the conductive body, there is a large anomaly at the lowest frequencies (<30 Hz) as a result of the charge distribution impinged upon the body by the ocean electrical currents and which can be misinterpreted as a large conductor.

Two-dimensional inversions of the data corresponding to the ocean + body model have been carried out. It is impossible for

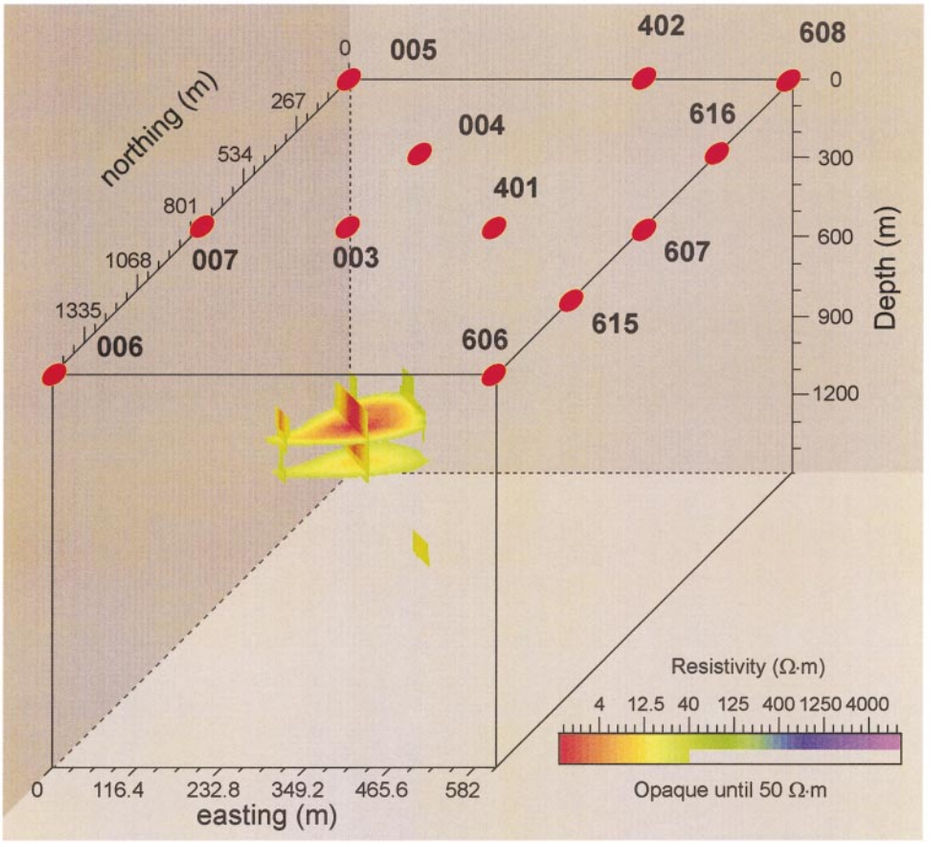


FIG. 19. Slices through the pseudo-3D model with resistivities above 50 ohm-m set to opaque.

the inversion scheme to reproduce correctly the TE-mode behavior, although the TM mode is easily modeled. The best inversions show a conductor of resistivity and dimensions higher than in the original model, and a second layer located under the conductor.

## CONCLUSIONS

This case study of AMT data over a small conductor has demonstrated a number of important aspects. With regard to data acquisition, high-quality data are required in the 1000–10 000 Hz range in order to (1) resolve better the structures in the top 500 m and (2) aid definition of static shifts on the AMT apparent resistivity curves. As emphasized by Garcia and Jones (2002), for the most optimum signal-to-noise ratio, these data must be acquired during night hours due to the attenuation of the magnetic fields from distant lightning sources in the enhanced sunlit atmospheric conductivity. Also, high-quality vertical magnetic field data leading to superior geomagnetic transfer response functions must be acquired over the whole bandwidth.

These data have demonstrated the requirement for careful data analysis and appraisal prior to modeling. The analysis is to determine the extent of galvanic distortions and the appropriate dimensionality, whereas the appraisal is to determine whether the data are internally self-consistent. For these data,

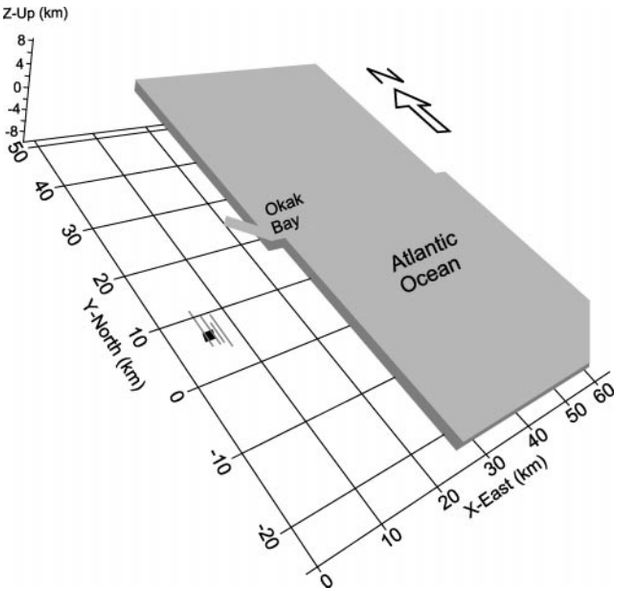


FIG. 21. Three-dimensional regional model including the Atlantic Ocean and Okak Bay, and also a representation of the minor anomaly studied herein.

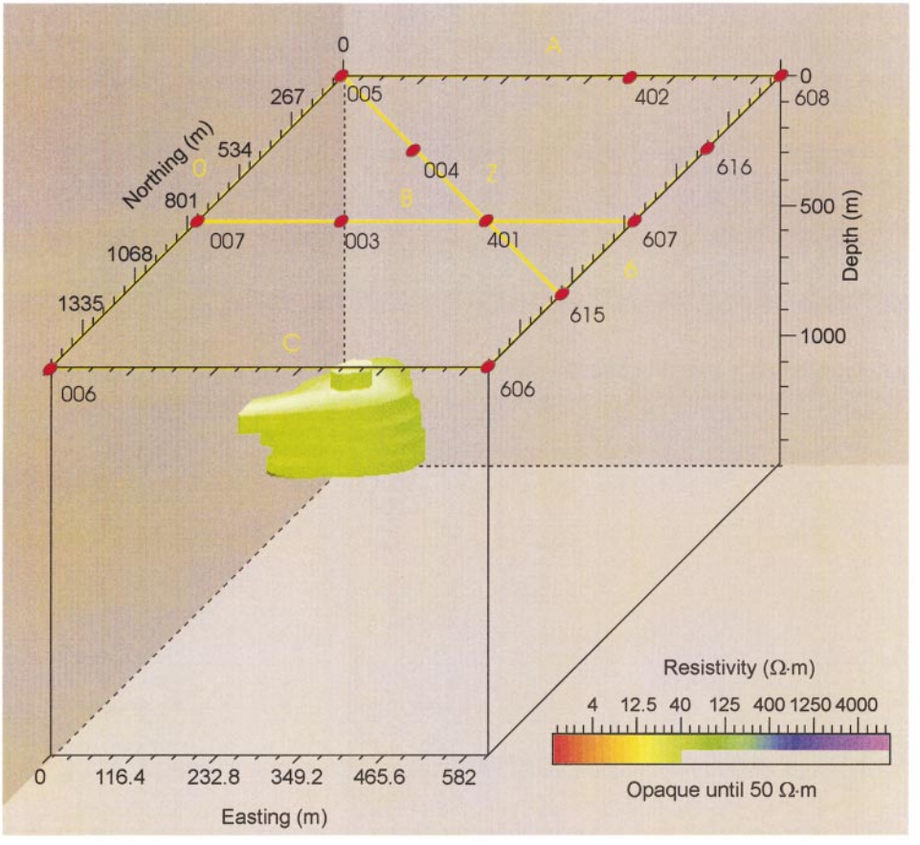


FIG. 20. Fifty ohm-meter surface of the pseudo-3D model.

the low-frequency decay in the apparent resistivity curves at all sites close to the anomaly cannot be validly interpreted using 2D codes.

Two-dimensional modeling of appropriate data over 3D mineralized bodies can yield geometrical and physical property information that are reasonably accurate and can be used for defining a drilling program to test the results. Once a single hole is drilled and conductivity information obtained by well logging, the inversions can be reperformed holding fixed the resistivity values in the model cells intersected by the trajectory of the borehole. Even minimal a priori information constrains inversions significantly (e.g., Kim et al., 1999) and, given the costs of drilling a borehole, the maximum use should be made of the knowledge obtained and applied to existing data.

With regard to the objective of the survey, mapping of the induction vectors and the distortion-corrected responses showed that there is only one anomalous conductor in the region, and that it is bounded roughly by the triangle formed by sites 004, 007, and 003. This anomaly is the one intersected by drillholes.

Two-dimensional inversions of the distortion-corrected data show the presence of a single minor conductor of about 2 S total conductance in the area located at depth between stations 005, 004, 003, and 007. Given that the body is 3D and not 2D, Martinelli et al.'s (2000) comparison study would suggest that we underestimate the conductance value by up to 30%, so to be conservative we assign a maximum vertically integrated conductance of about 3 S for the anomaly. This anomaly correlates with the mineralization intersected by the AMT-defined drilling program (OK-M1, OK-M2, and OK-M3), and the response of this conductor explains almost all of the observed AMT anomalies in the 1000–10 Hz frequency range. The drilled pyrrhotite in the 16.4-m depth interval between 454.1–470.5 m would explain this anomaly, and an average volume percent of 0.3% pyrrhotite is sufficient for the approximately 8-ohm-m inferred resistivity of the layer.

We find no evidence for any enhancement in conductivity beginning at a depth of approximately 1000 m as shown in the contractor's preliminary interpretation of the line 600 data (Figure 3). We suspect that this anomaly came from

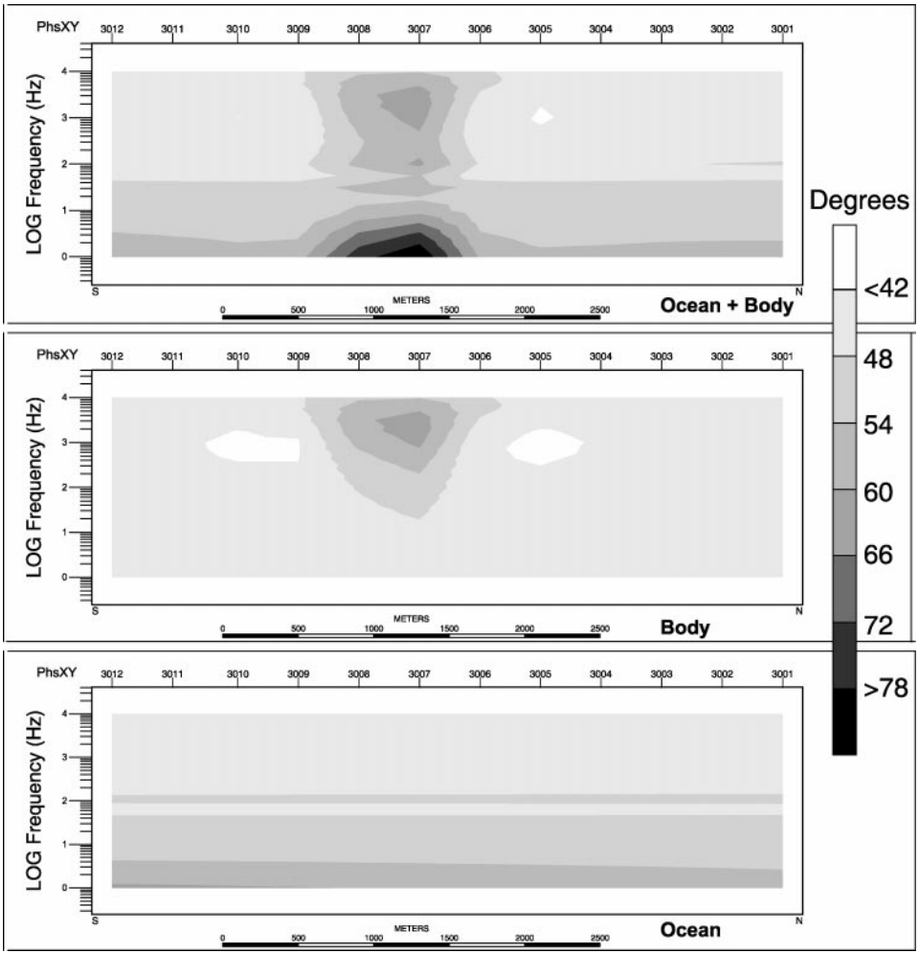


FIG. 22. Phase pseudosections for currents traveling east-west (regional TM mode) from the model shown in Figure 21. (Top) Both the ocean and the body are included, (middle) only the response of the body, and (bottom) only the response from the ocean.

interpreting the apparent resistivity data at frequencies below 10 Hz where there is a strong anomalous decay response. However, the data at these frequencies are significantly affected by the mutual interaction of off-profile structures, in this case the mineralized zone intersected by the boreholes and the electric currents in the ocean.

We have attempted to model the EM effects of the distant ocean. Although we are unable to reproduce the primary observations, the modeling does indicate that one should expect the low-frequency responses to be seriously affected, leading to the presence of a deeper false conductor. These effects can be avoided in the final 2D model by restricting the frequency range to use in the inversion. This, however, limits penetration significantly.

Using an interpolation algorithm and with the use of 3D plotting code, a final pseudo-3D model has been obtained showing the presence of a single conductor in the area. Although this is not a formal 3D model, the location and geometry provided from combining the 2D inversions are sufficient for exploration purposes.

Inversion of the data from station 005 demonstrates that the TEM conductor in time channel 0.55 ms has a counterpart in the AMT response. Although initial interpretation of the TEM data implied a conductor at a depth of 100–200 m, this can be rejected based on the AMT responses. The AMT data can be explained by the 3.5-m-thick zone of mineralization intersected at 523.6 m. Comparing the AMT and TEM responses for sites 005 and 004, we find perplexingly that even though the mineralization intersected is at approximately the same depths for OK-M2 and OK-M8, the AMT response is largest at site 004 and weaker at site 005, whereas the converse holds for the TEM data. We conclude that the TEM data are sensitive to concentrations of mineralization within a confined body, whereas the AMT data are more sensitive to interconnectivity over a larger region.

## ACKNOWLEDGMENTS

The authors thank Gallery Resources for making the Okak Bay AMT dataset available for interpretation and for partially financing the work presented here. Dr. Dennis Woods provided

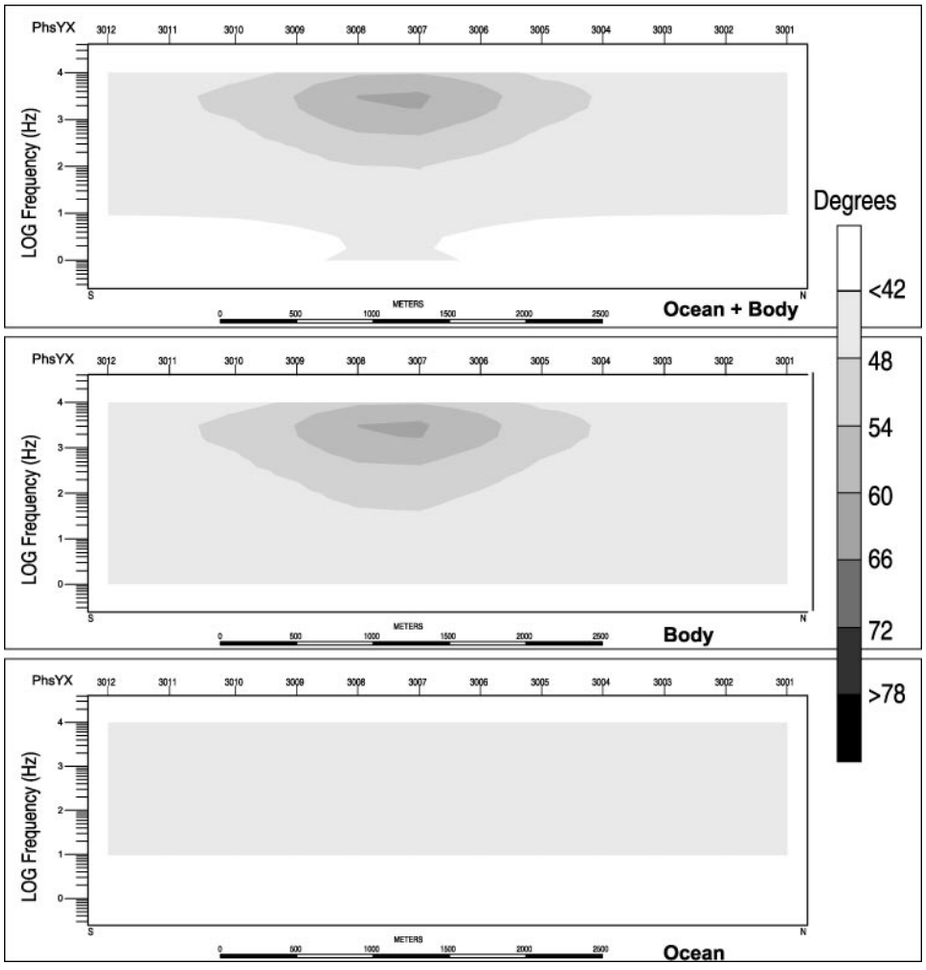


FIG. 23. Phase pseudosections for currents traveling north-south (regional TE mode) from the model shown in Figure 21. (Top) Both the ocean and the body are included, (middle) only the response of the body, and (bottom) only the response from the ocean.

a pivotal role in proposing this collaborative effort and in liaising between ourselves and Gallery Resources. Jim Craven, Colin Farquharson, and Ian Ferguson are thanked for their comments on an earlier version of this paper. X.G. was supported by an NSERC Research Fellowship funded by the Geological Survey of Canada, Phoenix Geophysics (Scarborough), Geosystem Srl. (Milan), and Inco Ltd. Geological Survey of Canada contribution number 2000131.

## REFERENCES

Agarwal, A. K., Poll, H. E., and Weaver, J. T., 1993, One- and two-dimensional inversion of magnetotelluric data in continental regions: Phys. Earth Planet. Inter., **81**, 155–176.

Bahr, K., 1991, Geological noise in magnetotelluric data: A classification of distortion types: Phys. Earth Planet. Inter., **66**, 24–38.

Balch, S., Crebs, T. J., King, A., and Verbiski, M., 1998, Geophysics of the Voisey's Bay Ni-Cu-Co deposits. 68th Ann. Internat. Mtg., Soc. Expl. Geophys., Expanded Abstracts.

Berdichevsky, M. N., and Dmitriev, V. I., 1976, Basic principles of interpretation of magnetotelluric sounding curves, *in* Adam, A., Ed., Geoelectric and geothermal studies: Akademiai Kiad, 165–221.

Cagniard, L., 1953, Basic theory of the magneto-telluric method of geophysical prospecting: Geophysics, **18**, 605–635.

Chave, A. D., and Jones, A. G., 1997, Electric and magnetic field distortion decomposition of BC87 data: J. Geomagn. Geoelectr., **49**, 767–789.

Chouteau, M., Zhang, P., Dion, D. J., Giroux, B., Morin, R., and Krivochieva, S., 1997, Delineating mineralization and imaging the regional structure with magnetotellurics in the region of Chibougamau (Canada): Geophysics, **62**, 730–748.

Constable, S. C., Parker, R. L., and Constable, C. G., 1987, Occam's inversion: A practical algorithm for generating smooth models from electromagnetic sounding data: Geophysics, **52**, 289–300.

Dawson, T. W., Weaver, J. T., and Raval, U., 1982, B-polarization induction in two generalized thin sheets at the surface of a conducting half space: Geophys. J. Roy. Astr. Soc., **69**, 209–234.

Edwards, R. N., Bailey, R. C., and Garland, G. D., 1981, Conductivity anomalies: Lower crust or asthenosphere? Phys. Earth Planet. Inter., **25**, 263–272.

Emslie, R. F., and Loveridge, W. D., 1992, Floride-bearing Early and Middle Proterozoic granites, Okak Bay area, Labrador: Geochronology, geochemistry and petrogenesis: Lithos, **28**, 87–109.

Ermanovics, I., Emslie, R. F., and Ryan, B., 1997, Geology of the Umiakovik Lake–Kiglapait Mountains, Labrador, Newfoundland. Scale: 1:100 000: Geological Survey of Canada Open File 3451.

Ermanovics, I., and van Kranendonk, M., 1998, Geology of the Archean Nain Province and Paleoproterozoic Torngat Orogen in a transect of the North River–Nutak map areas, Newfoundland (Labrador) and Quebec: Geological Survey of Canada Bulletin 497.

Fischer, G., and Le Quang, B. V., 1981, Topography and minimization of the standard deviation in one-dimensional magnetotelluric modelling: Geophys. J. Roy. Astr. Soc., **67**, 279–292.

Garcia, X., and Jones, A. G., 2002, Atmospheric sources for audio-magnetotelluric (AMT) sounding: Geophysics, **67**, 448–458.

Goldstein, M. A., and Strangway, D. W., 1975, Audio-magnetotellurics with a grounded electric dipole source: Geophysics, **40**, 669–683.

Groom, R. W., and Bailey, R. C., 1989, Decomposition of magnetotelluric impedance tensors in the presence of local three-dimensional galvanic distortion: J. Geophys. Res., **94**, 1913–1925.

———1991, Analytical investigations of the effects of near-surface three-dimensional galvanic scatterers on MT tensor decomposition: Geophysics, **56**, 496–518.

Groom, R. W., Kurtz, R. D., Jones, A. G., and Boerner, D. E., 1993, A quantitative methodology for determining the dimensionality of conductive structure from magnetotelluric data: Geophys. J. Internat., **115**, 1095–1118.

Habashy, T. M., Groom, R. W., and Spies, B. R., 1993, Beyond the Born and Rytov approximations: A nonlinear approach to electromagnetic scattering: J. Geophys. Res., **98**, 1759–1775.

Jones, A. G., 1982, On the electrical crust-mantle structure in Fennoscandia: No Moho and the asthenosphere revealed? Geophys. J. Roy. Astr. Soc., **68**, 371–388.

———1983, The problem of "current channelling": A critical review: Geophys. Surv., **6**, 79–122.

———1986, Parkinson's pointers' potential perfidy!: Geophys. J. Roy. Astr. Soc., **87**, 1215–1224.

———1992, Electrical conductivity of the continental lower crust, *in* eds., Fountain, D. M., Arculus, R. J., and Kay, R. W., Eds., Continental lower crust: Elsevier, 81–143.

———1993, The COPROD2 dataset: Tectonic setting, recorded MT data and comparison of models: J. Geomagn. Geoelectr., **45**, 933–955.

Jones, A. G., Craven, J. A., McNeice, G. A., Ferguson, I. J., Boyce, T., Farquharson, C., and Ellis, R. G., 1993, The North American Central Plains conductivity anomaly within the Trans-Hudson orogen in northern Saskatchewan: Geology, **21**, 1027–1030.

Jones, A. G., and Dumas, I., 1993, Electromagnetic images of a volcanic zone: Phys. Earth Planet. Inter., **81**, 289–314.

Jones, A. G., Katsube, J., and Schwann, P., 1997, The longest conductivity anomaly in the world explained: Sulphides in fold hinges causing very high electrical anisotropy: J. Geomagn. Geoelectr., **49**, 1619–1629.

Kim, H. J., Song, Y., and Lee, K. H., 1999, Inequality constraint in least-squares inversion of geophysical data: Earth Planets Space, **51**, 255–259.

Livelybrooks, D. W., Mareschal, M., Blais, E., and Smith, J. T., 1996, Magnetotelluric delineation of the Trillabelle massive sulfide body in Sudbury, Ontario: Geophysics, **61**, 971–986.

Martinelli, P., Osella, A., and Pomposiello, C., 2000, Comparative magnetotelluric modeling of smooth 2D and 3D conducting bodies using Rayleigh-Fourier codes: Pure Appl. Geophys., **157**, 383–405.

McNeice, G., and Jones, A. G., 2001, Multi-site, multi-frequency tensor decomposition of magnetotelluric data: Geophysics, **66**, 158–173.

Park, S. K., and Mackie, R. L., 1997, Crustal structure at Nanga Parbat, northern Pakistan, from magnetotelluric soundings: Geophys. Res. Lett., **24**, 2415–2418.

Parker, R. L., 1980, The inverse problem of electromagnetic induction: existence and construction of solutions based on incomplete data: J. Geophys. Res., **85**, 4421–4425.

Parker, R. L., and Booker, J. R., 1996, Optimal one-dimensional inversion and bounding of magnetotelluric apparent resistivity and phase measurements: Phys. Earth Planet. Inter., **98**, 269–282.

Parker, R. L., and Whaler, K. A., 1981, Numerical methods for establishing solutions to the inverse problem of electromagnetic induction: J. Geophys. Res., **86**, 9574–9584.

Parkinson, W. D., 1962, The influence of continents and oceans on geomagnetic variations: Geophys. J. Roy. Astr. Soc., **6**, 441–449.

Price, A. T., 1973, The theory of geomagnetic induction: Phys. Earth Planet. Inter., **7**, 227–233.

Ranganayaki, R. P., and Madden, T. R., 1980, Generalized thin sheet analysis in magnetotellurics: An extension of Price's analysis: Geophys. J. Roy. Astr. Soc., **60**, 445–457.

Rodi, W., and Mackie, R. L., 2001, Nonlinear conjugate gradients algorithm for 2-D magnetotelluric inversion: Geophysics, **66**, 174–187.

Ryan, B., Compiler, 1990, Preliminary geological map of the Nain Plutonic Suite and surrounding rocks (Nain-Nutak NTS 14 S.W.), scale 1:500,000: Geological Survey Branch, Dept. Mines, Energy, St. John's, Newfoundland, Map 90–44.

Schilling, F. R., Partzsch, G. M., Brasse, H., and Schwarz, G., 1997, Partial melting below the magmatic arc in the central Andes deduced from geoelectromagnetic field experiments and laboratory data: Phys. Earth Planet. Inter., **103**, 17–31.

Smith, J. T., and Booker, J. R., 1991, Rapid inversion of two and three-dimensional magnetotelluric data: J. Geophys. Res., **96**, 3905–3922.

Spies, B. R, 1989, Depth of investigation in electromagnetic sounding methods: Geophysics, **54**, 872–888.

Sternberg, B. K., Washburne, J. C., and Pellerin, L., 1988, Correction for the static shift in magnetotellurics using transient electromagnetic soundings: Geophysics, **53**, 1459–1468.

Stevens, K. M., and McNeice, G., 1998, On the detection of Ni-Cu ore hosting structures in the Sudbury Igneous Complex using the magnetotelluric method: 68th Ann. Internat. Mtg., Soc. Expl. Geophys., Expanded Abstracts.

Taylor, F. C., Compiler, 1977, Geology, North River–Nutak, Newfoundland-Quebec. Scale: 1:250 000: Geological Survey of Canada Map 1436A.

Taylor, F. C., Reinhardt, E. W., Froese, E., and Morgan, W. C., 1969, Geology of North River–Nutak area, Labrador, *in* Taylor, F. C., Compiler, Geology, North River–Nutak, New found land-Quebec. Scale: 1:250 000: Geological Survey of Canada Map 143.

Vozoff, K., 1972, The magnetotelluric method in the exploration of sedimentary basins: Geophysics, **37**, 98–141.

———1991, The magnetotelluric method, *in* Electromagnetic methods in applied geophysics—Applications: Soc. Expl. Geophys., 641–712.
Wannamaker, P. E., Hohmann, G. W., and Ward, S. H., 1984, Magnetotelluric responses of three-dimensional bodies in layered earths: Geophysics, **49**, 1517–1533.
Weidelt, P., 1972, The inverse problem of geomagnetic induction: Z. Geophys, **38**, 257–289.
Weidelt, P., and Kaikkonen, P., 1994, Local 1-D interpretation of magnetotelluric B-polarization impedances: Geophys. J. Internat., **117**, 733–748.
Wheeler, J. O., Hoffman, P. F., Card, K. D., Davidson, A., Sanford, B. V., Okulitch, A. V., and Roest, W. R., 1997, Geological Map of Canada: Geological Survey of Canada Map D1860A (ver 1.0).
Zhang, P., King, A., and Watts, D., 1998, Using magnetotellurics for mineral exploration: 68th Ann. Internat. Mtg., Soc. Expl. Geophys., Expanded Abstracts.